AD NUMBER

ADB275535

NEW LIMITATION CHANGE

TO

Approved for public release, distribution
unlimited

FROM

Distribution authorized to U.S. Gov't.
agencies only; Proprietary Info.; Sep
2001. Other requests shall be referred to
U.S. Army Medical Research and Materiel
Command, 504 Scott St., Ft. Detrick, MD
21702-5012.

AUTHORITY

USAMRMC ltr, 28 Aug 2002

AD_____

Award Number: DAMD17-00-1-0625

TITLE: Imaging Angiogenesis In Vivo: "Immunospecific" Magnetic Resonance Imaging of Breast Tumors Using Antibody-Coated Magnetite Particles

PRINCIPAL INVESTIGATOR: Paula J. Gareau

CONTRACTING ORGANIZATION: The John P. Robarts Research Institute
London, Ontario N6A 5K8 Canada

REPORT DATE: September 2001

TYPE OF REPORT: Final

PREPARED FOR: U.S. Army Medical Research and Materiel Command
Fort Detrick, Maryland 21702-5012

The views, opinions and/or findings contained in this report are those of the author(s) and should not be construed as an official Department of the Army position, policy or decision unless so designated by other documentation.

20020215 080

NOTICE

USING GOVERNMENT DRAWINGS, SPECIFICATIONS, OR OTHER DATA INCLUDED IN THIS DOCUMENT FOR ANY PURPOSE OTHER THAN GOVERNMENT PROCUREMENT DOES NOT IN ANY WAY OBLIGATE THE U.S. GOVERNMENT. THE FACT THAT THE GOVERNMENT FORMULATED OR SUPPLIED THE DRAWINGS, SPECIFICATIONS, OR OTHER DATA DOES NOT LICENSE THE HOLDER OR ANY OTHER PERSON OR CORPORATION; OR CONVEY ANY RIGHTS OR PERMISSION TO MANUFACTURE, USE, OR SELL ANY PATENTED INVENTION THAT MAY RELATE TO THEM.

LIMITED RIGHTS LEGEND

Award Number: DAMD17-00-1-0625
Organization: The John P. Robarts Research Institute

Those portions of the technical data contained in this report marked as limited rights data shall not, without the written permission of the above contractor, be (a) released or disclosed outside the government, (b) used by the Government for manufacture or, in the case of computer software documentation, for preparing the same or similar computer software, or (c) used by a party other than the Government, except that the Government may release or disclose technical data to persons outside the Government, or permit the use of technical data by such persons, if (i) such release, disclosure, or use is necessary for emergency repair or overhaul or (ii) is a release or disclosure of technical data (other than detailed manufacturing or process data) to, or use of such data by, a foreign government that is in the interest of the Government and is required for evaluational or informational purposes, provided in either case that such release, disclosure or use is made subject to a prohibition that the person to whom the data is released or disclosed may not further use, release or disclose such data, and the contractor or subcontractor or subcontractor asserting the restriction is notified of such release, disclosure or use. This legend, together with the indications of the portions of this data which are subject to such limitations, shall be included on any reproduction hereof which includes any part of the portions subject to such limitations.

THIS TECHNICAL REPORT HAS BEEN REVIEWED AND IS APPROVED FOR PUBLICATION.

_Kath___ Mor___ 2/4/02_ _____

_____ _____

REPORT DOCUMENTATION PAGE

Form Approved
OMB No. 074-0188

1. AGENCY USE ONLY (Leave blank)	2. REPORT DATE September 2001	3. REPORT TYPE AND DATES COVERED Final (01 Sep 00 - 31 Aug 01)	

4. TITLE AND SUBTITLE
Imaging Angiogenesis In Vivo: "Immunospecific" Magnetic Resonance Imaging of Breast Tumors Using Antibody-Coated Magnetite Particles

5. FUNDING NUMBERS
DAMD17-00-1-0625

6. AUTHOR(S)
Paula J. Gareau

7. PERFORMING ORGANIZATION NAME(S) AND ADDRESS(ES)

The John P. Robarts Research Institute
London, Ontario N6A 5K8 Canada

E-mail: pgareau@irus.rri.ca

8. PERFORMING ORGANIZATION REPORT NUMBER

9. SPONSORING / MONITORING AGENCY NAME(S) AND ADDRESS(ES)

U.S. Army Medical Research and Materiel Command
Fort Detrick, Maryland 21702-5012

10. SPONSORING / MONITORING AGENCY REPORT NUMBER

11. SUPPLEMENTARY NOTES
Report contains color

12a. DISTRIBUTION / AVAILABILITY STATEMENT
Distribution authorized to U.S. Government agencies only (proprietary information, Sep 01). Other requests for this document shall be referred to U.S. Army Medical Research and Materiel Command, 504 Scott Street, Fort Detrick, Maryland 21702-5012.

12b. DISTRIBUTION CODE

13. ABSTRACT (Maximum 200 Words)

The purpose of this research is to develop a non-invasive observation of angiogenesis through the design and validation of MRI pulse sequences and novel contrast agents and to use this agent to monitor angiogenesis in vivo over time during tumor development.
This is being achieved by the following:
1. Optimization of MR pulse sequence technology for the relative assessment of tissue iron concentrations based on the quantitative evaluation of T2 and T2* weighted images.
2. Development of novel, highly specific iron oxide based, magnetic resonance contrast agents to be used for targeting receptors and/or macrophage populations associated with tumor cells.

14. SUBJECT TERMS
Breast cancer, magnetic resonance imaging, angiogenesis, contrast agents

15. NUMBER OF PAGES
67

16. PRICE CODE

17. SECURITY CLASSIFICATION OF REPORT Unclassified	18. SECURITY CLASSIFICATION OF THIS PAGE Unclassified	19. SECURITY CLASSIFICATION OF ABSTRACT Unclassified	20. LIMITATION OF ABSTRACT Unlimited

NSN 7540-01-280-5500

Standard Form 298 (Rev. 2-89)
Prescribed by ANSI Std. Z39-18
298-102

Table of Contents

Introduction

Tumor progression depends on the ability to stimulate the development of new blood vessels.[1] This process is known as tumor angiogenesis. It has been hypothesized that the characteristic new vessel growth associated with tumor angiogenesis should allow differentiation between malignant and benign breast lesions. Recent studies point to vascular endothelial growth factor (VEGF) as a major regulator of physiological angiogenesis. VEGF is overproduced by tumor cells and acts predominantly as a potent angiogenic factor contributing to malignant progression.[2] The VEGF receptors are specifically expressed in the cell surface of vascular endothelial cells. Benign and malignant tumors are characterized by differential cellular expression of VEGF. Monitoring the expression of VEGF receptors may therefore be a reliable marker of the proliferative status of tumors.

Attempts to improve tumor detection by non-radioactive magnetic resonance imaging (MRI) techniques have led several investigators to develop "immuno-specific" paramagnetic contrast agents. We propose that the use of a magnetic label with high affinity and selectivity for VEGF receptors will allow VEGF-induced microvascularity to be visualized non-invasively using MRI.

The concept of this research is to develop a non-invasive observation of angiogenesis through the design and validation of MRI pulse sequences and novel contrast agents and to use this agent to monitor angiogenesis *in vivo* over time during tumor development.

The **specific objectives** are:

1. To develop novel, highly specific iron oxide based, magnetic resonance contrast agents to be used for targeting the macrophage population associated with tumor cells.

2. To optimize MR pulse sequence technology for the relative assessment of tissue iron concentrations based on the quantitative evaluation of T2 and T2* weighted images.

Body

Characterization of Breast Tumor Animal Model (Phase I)

The first phase of this research involved characterizing the histologic and MRI appearance of mammary tumors in the chosen animal model.

Breast tumors were induced in 30-day-old female Sprague Dawley rats by intraperitoneal (i.p.) injection of the carcinogen N-ethyl-N-nitrosurea (ENU: Isopack, Sigma Chemicals, St. Louis, MO). ENU is known to be a potent carcinogen that induces well vascularised mammary tumors in rats.[3] This tumor model was chosen because a range of benign and malignant tumors develop depending on the dose of ENU administered and because the tumor morphology and angiogenic behavior closely mimic breast tumors in humans. ENU was injected at two different doses: 40 mg/kg (n=20) and 180 mg/kg (n=20). Animals were visually checked for tumor growth ever second day. Once tumors were identified their size was tracked weekly using calipers. Tumors were imaged once they reached a size of at least 4 cm. Animals were anesthetized for MRI with ketamine/xylazine (10/100 mg/kg, i.p.). High-resolution *in vivo* MR images were obtained of all mammary tumors. After imaging animals were sacrificed and the tumors removed for histopathologic analysis. Photographs of the position of the tumors in the mammary tissue were obtained at post mortem to guide the correlating of MR and histologic images.

Tumors appeared as early as 60 days post ENU administration. In the low dose group (40 mg/kg) only 6/20 rats developed mammary tumors by 100 days post ENU administration. All 6 of these tumors were classified as benign. In the high dose group (180 mg/kg) 19/20 rats developed mammary tumors; 12 animals developed multiple

6

mammary tumors, in total 44 tumors were removed and examined. Of the 44 tumors from this high dose group, 35 were classified as malignant and 9 were classified as benign. Based on the results of this experiment further studies used only the high dose (180 mg/kg) of ENU since this protocol provided a useful spectrum of tumor types for analysis.

The appearance of benign mammary tumors in the MR images was typically of a consistent nature. Benign tumors appeared to have homogeneous signal intensity throughout. Tumor nodules were clearly visualized. The MRI appearance of malignant tumors was more variable. Malignant tumors often appeared to have a localized region of very low signal intensity that represented a necrotic core. Based on the results of this analysis the tumor type and regions of tumor anatomy could be recognized *in vivo* by MRI.

Pulse Sequence Development (Phase II)

The second phase of this project involved MRI pulse sequence and software analysis development. This work was critical to the concept of quantifying iron content *in vivo* using noninvasive MRI techniques. This phase of research was done in collaboration with Dr. Brian Rutt's group, a collaborator in the Imaging Research Lab.

3D multi-echo gradient echo and spin echo (CPMG) sequences have been developed and implemented in our lab (detailed descriptions of the pulse sequence development and testing can be found in the appended manuscript ("Application of Static Dephasing Regime Theory to Superparamagnetic Iron-Oxide Loaded Cells"). These

experiments have resulted in the submission and acceptance of a manuscript that is currently being revised for publication (see Appendix).

In Vitro Cell Studies (Phase III)

The third phase of this work involved an examination of iron uptake by phagocytic cells. In invasive breast cancers, the neoplastic cell population is often outnumbered by stromal cells, such as the tumor associated macrophage (TAM),[4] a mononuclear cell of the inflammatory system. It is thought that monocytes in the peripheral circulation are actively recruited to the tumor site. Once recruited, the monocytes differentiate to become TAMs. The role of TAMs in breast tumor tissue is not completely understood. In the tumor microenvironment TAMs are modified to secrete growth factors such as EGF, VEGF, TNFα and bFGF.[5] It has been suggested that TAMs play a role in neovascularization, are related to angiogenesis, and ultimately survival and proliferation of the tumor cell population.[6]

An imaging method that can define the extent of this activity would have a significant impact on cancer imaging and research. Since macrophages ingest iron oxide particles we investigated the application of optimized imaging methods from Phase II for measuring iron oxide uptake into phagocytic cells.

In vitro experiments have demonstrated our ability to measure iron oxide uptake into a macrophage-like cell line and to characterize uptake efficiency as a function of particle size, dose and incubation time. The results of these experiments indicate that (i) R2*is more than 100 times more sensitive than R2 to iron based contrast agents compartmentalized in cells, (ii) iron uptake by phagocytic cells is linear, we have defined

a parameter for uptake efficiency (dose*time) which allows the uptake efficiency to be defined for any cell type and contrast agent (see Figure 1), and (iii) iron within cells is quantifiable using R2′ mapping. R2′ is directly proportional to iron concentration when compartmentalized within cells (see Figure 2). This data is included in the submitted manuscript.

In Vivo Animal Studies (Phase IV)

In the fourth phase of this research project MR techniques, developed in *Phase II* and testing *in vitro* in *Phase III*, are applied to study the mammary tumor in live rats. theoretical estimates of R_2', developed in *Phase II*, are extended to predict the *in vivo* detection threshold of iron-oxide in cells.

Images were acquired of both mammary tumor tissue and normal brain, as examples of highly homogeneous and heterogeneous tissue types, respectively. For imaging studies rats were anesthetized with an intraperitoneal injection of ketamine/xylazine (100/10 mg/kg) and positioned supine within a 5 cm diameter solenoid RF coil in a 4 T Varian/Siemens whole body scanner. Axial R_2^* maps of both rat brain and tumor were generated using the 3D multi-echo gradient echo sequence (256x256, 32 slices at 250 mm resolution, 6 cm FOV, 77 kHz full receive bandwidth, 120 ms TR, 30° flip angle). Separate image volumes were produced for each of 14 echoes acquired using a 4 ms echo spacing. R_2 maps were acquired using a single slice 2D multi-echo CPMG sequence (192x192, 4 mm slice, 6 cm FOV, 74 kHz full receive bandwidth, 3 second TR, 16 echoes with 7.5 ms echo spacing). Separate images, zero padded to 256x256, were produced for each echo, and the maximum echo time was acquired at TE_{max} = 120 ms (9.5 minutes per acquisition). Generation of R_2^* and R_2 maps from the corresponding multi-

9

echo gradient echo and CPMG images was accomplished using a 2 parameter mono-exponential fit for each pixel. The single slice for the 2D CPMG acquisition was positioned at the axial center of the 3D gradient echo volume for comparison with the R_2^* maps. R_2' maps were generated by subtracting the R_2^* value for each voxel in the 3D volume from the R_2 value of the corresponding in-plane pixel of the single slice R_2 map. While this method has some disadvantages due to partial volume effects relative to the acquisition of a full 3D CPMG volume, the approach was considered adequate since little variation in the axial direction was observed for the gradient echo images along the 4 mm range of the 2D slice. The results of these studies are shown in Figures 3-6.

Contrast Agent Development (Phase V)

We have investigated the use of iron oxide nanoparticles as a contrast agent for characterization and quantification of angiogenesis in mammary tumors. In attempt to further increase the specificity of MR contrast agents, superparamagnetic particles can be linked to monoclonal antibodies (MAbs), proteins or other target-specific moieties. The original goal of this work is to next examine iron oxides that have been conjugated to monoclonal antibodies, specifically antibodies directed against the VEGF receptor that is up regulated in tumor tissue. We have successfully developed the advanced MRI techniques, which are necessary to accurately resolve and quantify iron content, and so are well suited to explore the next phase of this research. We have developed research collaboration with Dr. Lee Josephson, a world expert in iron oxide based contrast agent development at the Center for Molecular imaging research at MGH.

Key Research Accomplishments

- Implementation and characterization of a carcinogen-induced (ethyl-N-nitrosourea) breast tumor model in rats that produces mammary tumors with a range of malignancies, from benign to malignant.

- Implementation and optimization of MRI pulse sequence technology (multi-echo 3D gradient echo and spin echo sequences) for iron assessment.

- Design and coding of computer programs that allow automated analysis of the MR images for the calculation of susceptibility and R2′ maps for determining iron content.

- *In vitro* cell studies: Analysis of the effect of particle size, incubation time and concentration of iron oxide nanoparticles on cellular uptake by phagocytic cells.

- *In vivo* animal studies: Analysis of the particle size, dose and time from injection of iron oxide nanoparticles on iron uptake in TAMs.

- Correlative analysis of MR and histologic images

The stated objective of developing more specific contrast agents for visualization of tumor microvasculature has not been accomplished at this time. This phase of the research has not begun yet; this is a reflection of the short term of this award. We are well suited to move forward with this component of the research, however, and plan to submit a grant application to the U.S. Army for funds to continue this research. Intermediary support has been provided by The Canadian Breast Cancer Research Initiative (see *Funding* below).

<u>Reportable Outcomes</u>

<u>Presentations and Publications</u>

1. The implementation and optimization of pulse sequence technology for iron assessment was presented as a poster at the 9th Meeting of the International Society for Magnetic Resonance in Medicine (ISMRM: Glasgow, 2001) and a manuscript relating to this work has been accepted for publication in *Magnetic Resonance in Medicine*. These publications are appended.

2. A second manuscript describing the application of these methods to the ENU tumor model is in preparation. This will also be prepared as an abstract for presentation at the 10th Meeting of the International Society for Magnetic Resonance in Medicine (ISMRM: Honolulu, 2002).

<u>Funding</u>

An IDEA Award (one year, $50,000) from the NCIC (Canadian Breast Cancer Research Initiative) has been awarded to Dr. Paula Gareau to continue the research supported by this grant.

Conclusions

The aim of this Concept Award was to study tumor angiogenesis in breast cancer, and the relationship to VEGF and TAMs, using advanced MRI techniques. To study these features of breast cancer pathology requires a method that is *noninvasive* and will allow frequent and repetitive observations in the same tumor over time during tumor development. Furthermore, the imaging method should be *specific* (to the TAM or VEGF receptors), *sensitive* to allow accurate, quantitative measurements, and of *high-resolution* to permit visualization of the microanatomical structure of the developing tumor.

With the support of this Concept Award, MRI pulse sequence technology has been developed and optimized for the relative assessment of tissue iron concentrations based on the quantitative evaluation of T2 and T2* weighted images. These methods allow high-resolution MR images to be obtained in a 3D format. Computer programs were written for the automated analysis of the MR images for the calculation of susceptibility and R2′ maps for determining iron content. These pulse sequence and software developments were validated *in vitro* in a cell preparations and *in vivo* in an ENU-induced mammary tumor model. We have defined a parameter for uptake efficiency (dose*time) that allows the uptake efficiency to be defined for any cell type and contrast agent. Iron oxide nanoparticles were studied for use as MRI contrast agents for imaging TAMs in mammary tissue. We have successfully developed MRI techniques, which are necessary to accurately resolve and quantify iron content *in vivo* and are prepared to investigate the next phase of this research.

Assessing the role of the TAM in tumor angiogenesis and tumorigenesis using this approach may result in novel *in vivo* markers for tumor type, aggressiveness and tumor margin delineation. Furthermore, the association of novel contrast agents with VEGF receptors, TAMs and/or phagocytosis of contrast agents by TAMs, forms the basis of a potential therapeutic strategy in which the contrast agent could serve as a targeted carrier of drugs.

References

1. Folkman J. What is the evidence that tumors are angiogenesis dependent? J Nat Cancer Inst 82, 4-6 (1990).

2. Carmeliet P and Jain RK. Angiogenesis in cancer and other diseases. Nature 407, 249-257 (2000).

3. Stoica G, Koestner A and Capen CC. Chracterization of N-ethyl-N-nitrosourea-induced mammary tumors in the rat. Am J Path 110, 161-169 (1983).

4. Dougherty ST, Eaves CJ, McBride WH, and Dougherty GJ. Role of macrophage-colony-stimulating factor in regulating the accumulation and phenotype of tumor-associated macrophages. Cancer Immunol Immunother 44, 165-172 (1997).

5. Leek RD, Lewis CE, Whitehouse R, Greenall M, Clarke J, and Harris AL. Association of macrophage infiltration with angiogenesis and prognosis in invasive breast carcinoma. Cancer Res 56, 4625-4629 (1996).

6. Sunderkotter C, Steinbrink K, Goebeler M, Bhardwaj R and Sorg C. Macrophages and angiogenesis. J Leukoc Biol 55, 410-422 (1994).
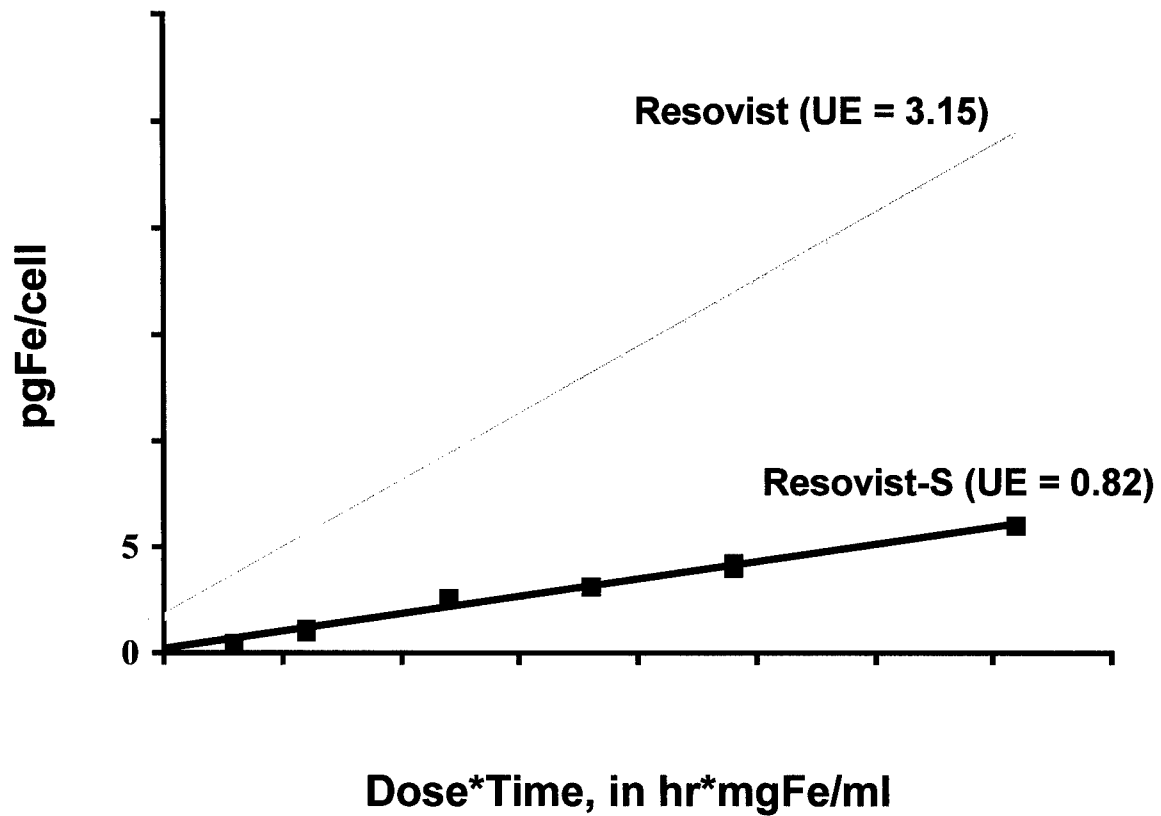
Appendix

Figure 1: Cellular uptake of two different sized iron oxide contrast agents:Resovist® (60nm) and Resovist-S® (20nm). The slope of the line represents the uptake efficiency (UE). Uptake by phagocytosis is linear so a unique uptake efficiency is defined for every cell and contrast agent
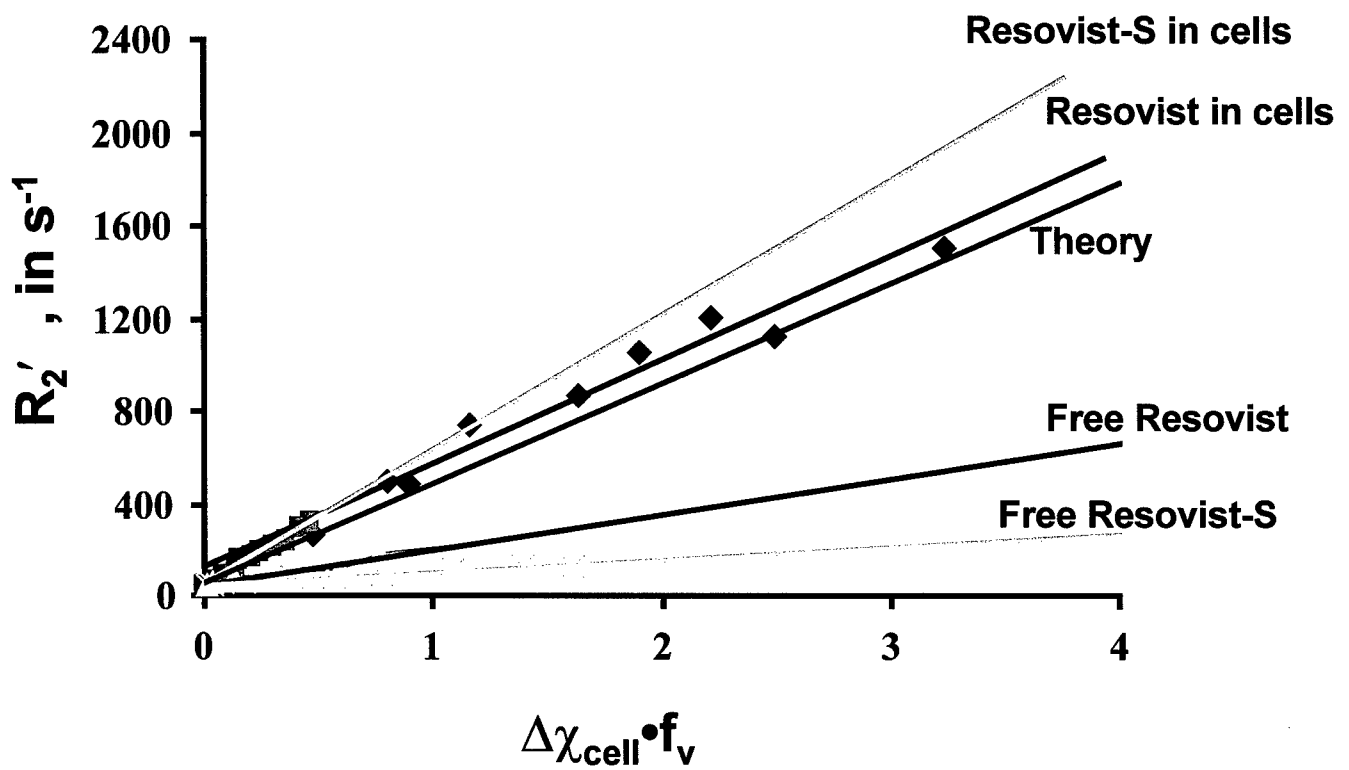
Figure 2: R_2' relaxivity at 4 Tesla. Experiments with different sized iron oxide contrast agents (Resovist=60nm, Resovist-S=20nm) in phagocytic cells or free in solution. R_2' is *independent* of contrast agent (or field strength) when compartmentalized in cells.
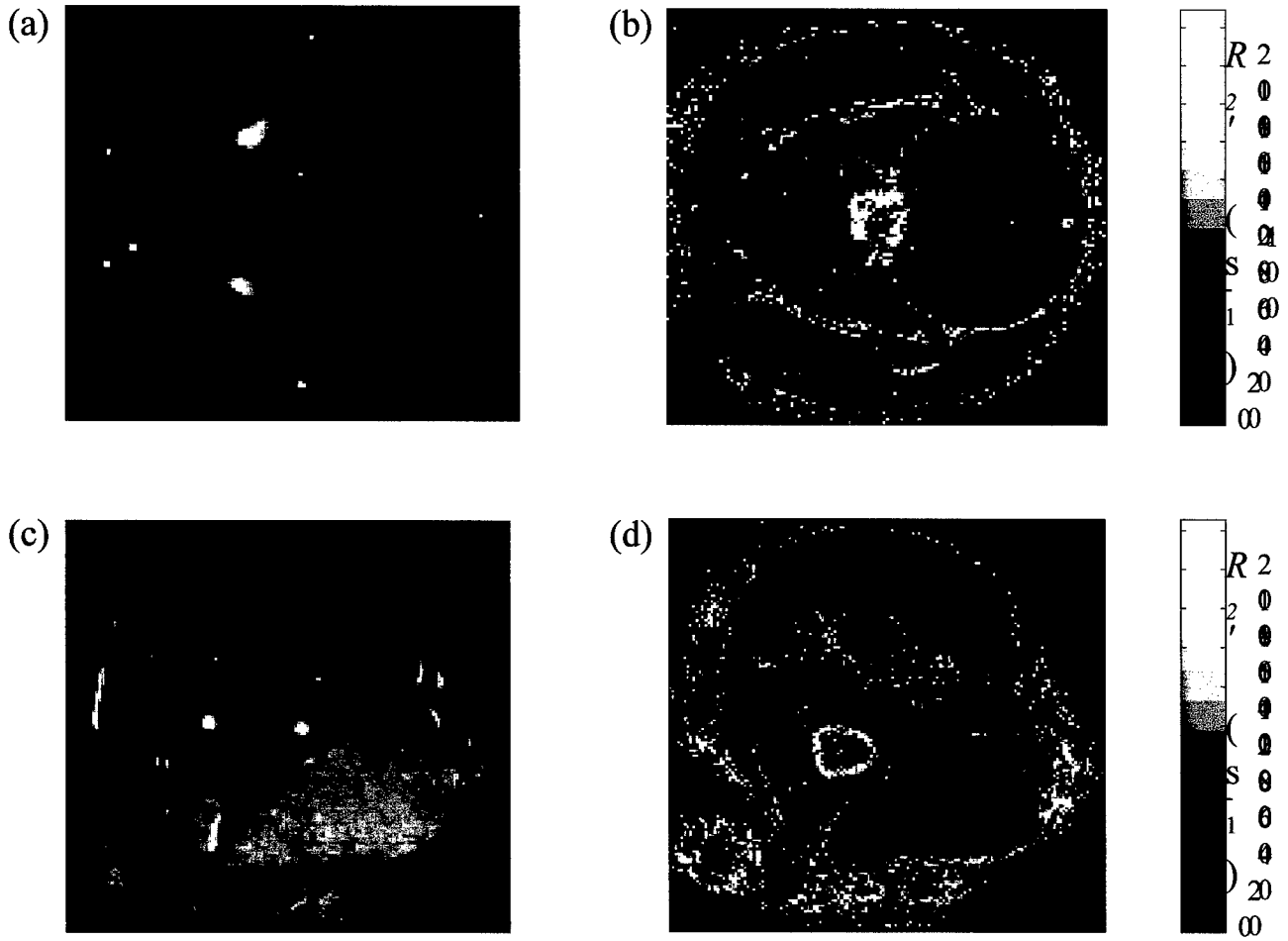
Figure 3: Example gradient echo images and R_2' maps from rat brain (**a,b**) and tumor (**c,d**). 3D multi-echo gradient echo images are of the first echo (4.5 ms *TE*). Dashed square indicates typical ROI selected for background R_2' analysis. Grayscale bars (0 to 200 s⁻¹) for R_2' maps (**b,d**) are identical.
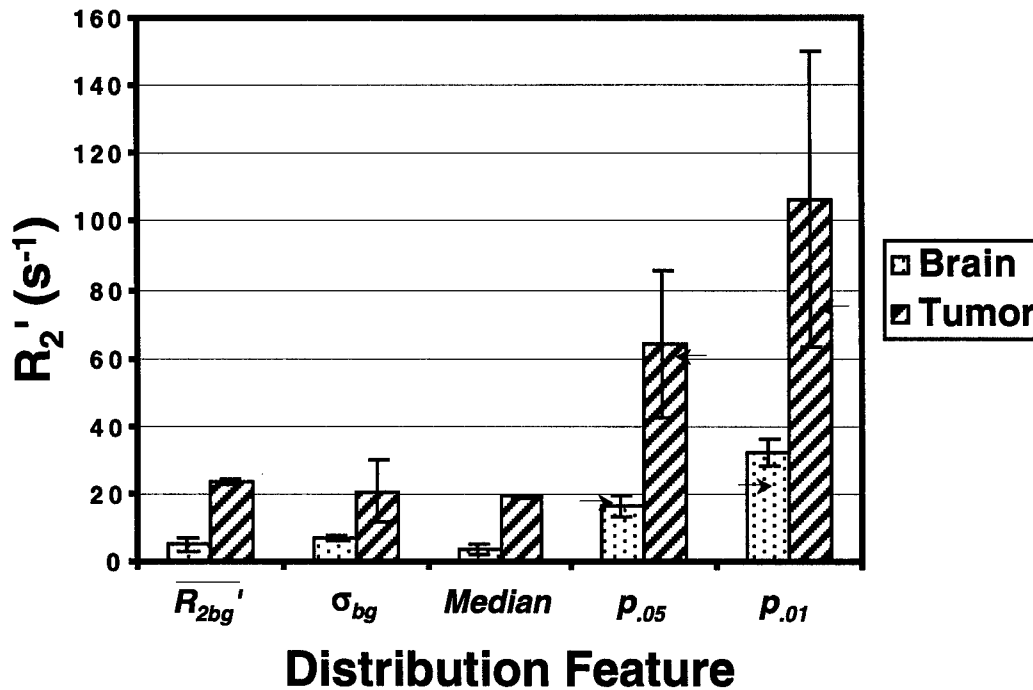
Figure 4: Summary of *in vivo* background R_2' distribution parameters for rat tumor and brain. Bar chart indicates background R_2' mean (R_{2bg}'), standard deviation (σ_{bg}), median, and the R_2' threshold greater then 95% ($p_{.05}$) and 99% ($p_{.01}$) of all R_2' values within the ROI. Data is averaged for 3 animals and error bars indicate the 95% confidence interval. Small arrows indicate normal distribution predictions of $p_{.05}$ and $p_{.01}$ based on the reported mean (R_{2bg}') and standard deviation (σ_{bg}). Agreement between the mean and median values reflects distribution symmetry. Agreement between the arrows and the measured p values indicates normally distributed R_2' values.

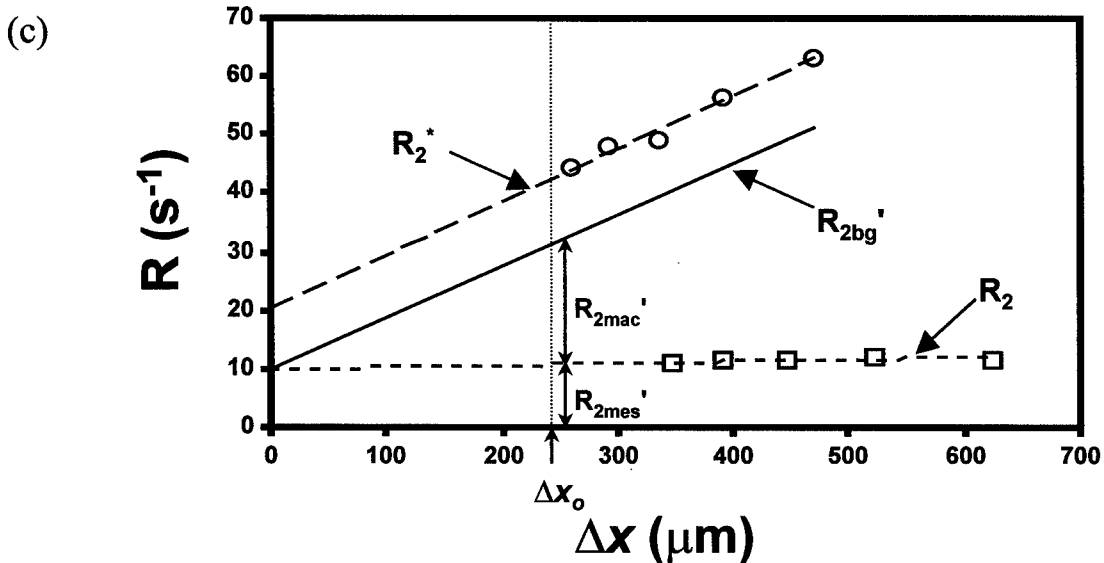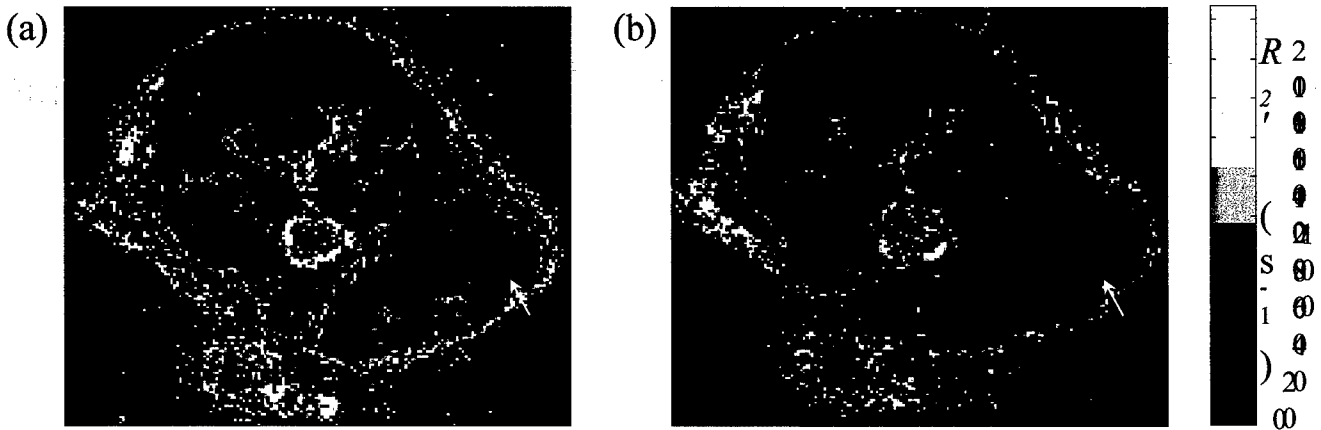Figure 5: Method for separating mesoscopic (R_{2mes}') and macroscopic (R_{2mac}') components of background R_2' (R_{2bg}'). Maps of R_{2mes}' (a) and R_{2mac}' (b) from rat tumor generated using the method illustrated in (c). The plot (c) shows relaxation rate dependence on pixel size for a single pixel from a portion of the tumor having a large macroscopic R_2' component (white arrows in (a) and (b)). The resolution dependence of R_2^* (circles) and R_2 (squares) is shown along with the linear fit for each (dashed and dotted line, respectively). R_{2bg}' (solid line) is derived from subtraction of the R_2^* and R_2 fitted curves. R_{2mes}' and R_{2mac}' at the gradient echo acquisition resolution (Δx_o) is indicated (see Eq. [3.3]). Maps of R_{2mac}' (b) have little fine structure and correlate with regions of large scale field inhomogeneity while R_{2mes}' maps (a) correlate with local tissue properties.
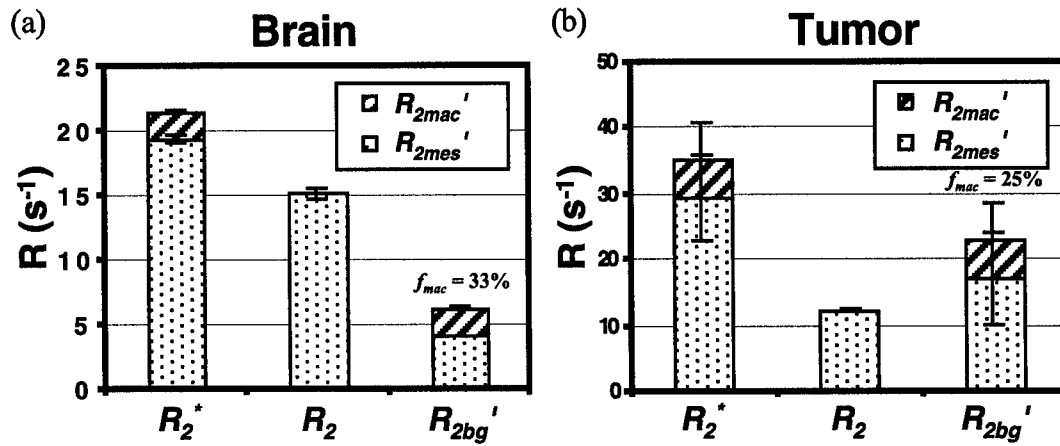
Figure 5: Summary of rat brain and tumor relaxation rates separated into mesoscopic and macroscopic components. The mesoscopic (dotted bar) and macroscopic (angled line bar) components of R_2^*, R_2 and R_{2bg}', measured using the method described in Fig. 4, are shown for the brain (a) and tumor (b) ROI. Note the different scale on the axis. Data is averaged for 3 animals and error bars indicate the 95% confidence interval. The fractional component of background R_2' (f_{mac}) at the gradient echo acquisition resolution ($\Delta x_o = 234$ μm) is 33% and 25% for rat brain and tumor, respectively.

MAGNETIC RESONANCE IN MEDICINE

Editor in Chief:
Felix W. Wehrli, Ph.D.

Editorial Assistant:
Colleen Flood

University of Pennsylvania Medical Center
Department of Radiology
3400 Spruce Street
Philadelphia, PA 19104-4283
Telephone: (215) 662-7951
FAX: (215) 349-5925
E-MAIL   MRM@oasis.rad.upenn.edu

Dr. Brian K. Rutt
Imaging Research Labs
John P. Robarts Research Institute
London, Ontario N6A 5K8ᵈʳⁱᵛᵉ
Canada

October 23, 2001

Re: MRM-101-5416

Dear Brian,

Your manuscript entitled:
Application of static dephasing regime theory to superparamagnetic iron-oxide loaded cells
has been reviewed.
All three referees are favorable and recommend further consideration with eventual publication. I concur with their assessments and am delighted to invite you to submit a revised manuscript, which must be received within 6 months from the date of this letter and which must effectively address the referees' critiques.

The manuscript is currently too long and needs to be shortened by 25%. Please provide a word count for before and after shortening.

Please make sure that the manuscript fully conforms in style and format to the Information for Authors section of the journal and its supplement, the MRM Style Guide, which is available for download at http://www.interscience.wiley.com/jpages/0740-3194/authors.html (click the "Style Guide" link) and is published in the first issue of every volume of the journal.

We urge you to submit the revision in the form of a PDF attachment to MRM@oasis.rad.upenn.edu, which will considerably speed up the review process. You may also send the revision in hard copy form. Either way, please submit a manuscript that is annotated by underlining the changes made and numbering them by referee and critique point number using marginal annotations. Further, please include a cover letter with a point-by-point list of how you have addressed the critiques, which will be forwarded to the referees along with the revised manuscript.

Please do **NOT** send diskettes or the copyright form with your revision. If your paper is accepted, you will be instructed to send the disks and a set of original figures to the publisher.

Sincerely,

Felix W. Wehrli, Ph.D.
Editor in Chief, Magnetic Resonance in Medicine

Application of Static Dephasing Regime Theory to Superparamagnetic Iron-Oxide Loaded Cells

Chris V. Bowen[1,3], Xiaowei Zhang[3], George Saab[1], Paula J. Gareau[1,3] and Brian K. Rutt[1,2,3]

[1]Department of Medical Biophysics and [2]Department of Diagnostic Radiology and Nuclear Medicine, University of Western Ontario, London, Ontario, Canada.
[3]Imaging Research Laboratories, The John P. Robarts Research Institute, London, Ontario, Canada.

Address correspondence to:

Dr. Brian K. Rutt, Ph.D.
Imaging Research Laboratories
The John P. Robarts Research Institute
P.O. Box 5015, 100 Perth Drive
London, Ontario, Canada
N6A 5K8
Phone: (519) 685-8300 x33408
Fax: (519) 663-3403
E-Mail: brutt@irus.rri.ca

Short Running Head:
Relaxivity of Iron-Oxide Loaded Cells

Contents List:
Text pages: 42
Figures: 7
Tables: 3

Abstract:

The relaxation rates of iron-oxide nanoparticles compartmentalized within cells were studied and found to satisfy predictions of static dephasing (SD) regime theory. THP-1 cells in cell culture were loaded using 2 different iron-oxide nanoparticles (SPIO and USPIO) with 4 different iron concentrations (0.05, 0.1, 0.2, 0.3 mg/ml) and for 5 different incubation times (6, 12, 24, 36, 38 hours). Cellular iron-oxide uptake was assessed using a newly developed imaging version of MR susceptometry and found to be linear with both dose and incubation time. R_2^* sensitivity to iron-oxide loaded cells was found to be 70 times greater than for R_2 and 3100 times greater than for R_1. This differs greatly from uniformly distributed nanoparticles and is consistent with a cellular bulk magnetic susceptibility relaxation mechanism. Cellular magnetic moment was large enough that R_2' relaxivity agreed closely with SD regime theory predictions for all cell samples tested. Uniform suspensions of SPIO and USPIO produced R_2' relaxivities that were a factor of 3 and 8 less than SD regime theory predictions, respectively. These results are consistent with theoretical estimates of the required mass of iron per compartment needed to guarantee SD-regime-dominant relaxivity. For cellular samples, R_2 was shown to be dependent on both the concentration and distribution of iron-oxide particles, while R_2' was sensitive to iron-oxide concentration alone, being independent of both field strength and particle size. This work is an important first step in quantifying cellular iron content and ultimately mapping the density of a targeted cell population.

2

Introduction

The macrophage is a white blood cell of the immune system which is intimately involved in the development and progression of inflammatory disease (1). Knowledge of the time course, spatial distribution and magnitude of inflammatory response, as well as the evolution of macrophage activation state, is critical for understanding disease progression (2,3). Currently, the most common method for assessing the extent of inflammation, or the effectiveness of various therapeutic strategies that inhibit inflammation, involves a histopathologic evaluation of multiple tissue sections. Imaging methods that are capable of defining the extent of inflammatory activity *in vivo* would have a significant impact on inflammation research.

It has recently become possible to visualize macrophage cells *in vivo*. Weissleder and colleagues have pioneered this development, utilizing iron oxide nanoparticles to image cellular uptake and trafficking by MRI (4). This technique exploits the ability of certain cell types to ingest small particles in culture and *in vivo* through phagocytosis. For example, intravenously administered iron oxide particles accumulate in macrophages of acute lesions in experimental autoimmune encephalomyelitis (5), and in tumor cells (6). While many papers report sensitivity to the presence of iron-oxide using T_1 (6,7), T_2 (5,8) and T_2^* (9,10) weighted imaging, methods quantifying the concentration of iron-oxide *in vivo*, as a first step towards characterizing the *degree* of inflammatory cell infiltration, are still lacking. The question of which acquisition strategy is the most sensitive and, in particular, the most accurate for quantifying the amount of iron-oxide compartmentalized within cells is, thus, still an open one. We have investigated, both theoretically and experimentally, the relaxation mechanism responsible for NMR signal decay in

the presence of iron-oxide nanoparticles, both in uniform suspension and following uptake into cells. Our results represent an important first step toward quantifying the cellular iron content and ultimately mapping the density of the targeted cell population.

Theory

Iron-oxide nanoparticles are superparamagnetic (SPM) particles (11), with magnetic moments more than 3 orders of magnitude greater than those of paramagnetic contrast agents (12). The quantitative dependence of both R_1 and R_2 (inverse T_1 and T_2) has been estimated using the Solomon-Bloembergen-Morgan equations, modified for the case of SPM particles, by Koenig (13), Bulte (12) and others. Below 1 T, these traditional quantum solutions describing electron-proton dipolar relaxation are quite successful in quantifying R_1 and R_2 relaxation rates for iron-oxide particles suspended in gel. SPM particles are observed to have a much smaller effect on T_1 then on T_2 relaxation compared to the effects produced by paramagnetic agents, owing to the large SPM magnetic moment.

However, when SPM particles are compartmentalized within cells rather than uniformly suspended in gel, the quantum solution fails. This effect has been observed both *in vivo*, for SPM particles sequestered within Kupffer cells of the reticuloendothelial system of the liver (14), and *in vitro*, in cell culture (4). In these studies, the ratio of R_2^* to R_2 is seen to increase dramatically compared to that observed in gel suspension, where the quantum solution would predict identical values for R_2^* and R_2. The quantum solution relies on the extreme motional narrowing approximation, which states that water diffusion between SPM particles occurs on a much shorter time scale than the peak resonant frequency offset. When iron-oxide particles are

compartmentalized, as within cells for instance, the cellular scale bulk magnetic susceptibility (BMS) effects produce dipolar field inhomogeneities large enough to violate this assumption. Unfortunately, no analytic solution describing R_1 or R_2 exists in this large perturber case (15), though Monte Carlo simulations of water diffusing through the BMS induced dipolar fields are quite successful in predicting R_2 and R_2^* (16-20).

Monte Carlo predictions, though useful for understanding the dominant relaxation mechanism, are difficult to generalize for differences in compartment size, field strength and pulse sequence parameters such as refocusing pulse spacing. However, an analytic solution does exist when perturber strength becomes large enough to satisfy the static dephasing (SD) regime condition (21,22). In this regime, the large compartmental magnetic moment produces a strong enough outer sphere dipolar field such that diffusion has no effect on the NMR signal decay. In the limit of the SD regime, R_1 and R_2 enhancement due to the presence of SPM particles approaches zero (15), while R_2', as predicted by Yablonskiy and Haacke (22) in Eq. [58] of their work, is given by the following relation (converted to SI units):

$$R_2' = \gamma \frac{2\pi}{9\sqrt{3}} \cdot LMD \qquad [1]$$

where γ is the proton gyromagnetic ratio and LMD is the local magnetic dose, defined by Yablonskiy and Haacke, as the tissue averaged magnetization difference due to the presence of SPM particles. By this formalism, $LMD \equiv f_v \cdot M_c$ where f_v is the fractional volume occupied by the magnetic compartments (cell volume fraction for instance) and M_c is the internal magnetization of the compartment due to the presence of SPM particles. R_2' is defined as $R_2^* - R_2$. In this case,

R_2' reflects the enhanced relaxation rate observed with gradient echo acquisitions due to the presence of SPM particles.

The conditions for which the outer sphere static dephasing regime equation, Eq. [1], accurately predicts R_2' relaxation is also indicated by Yablonskiy and Haacke. This SD regime limit is given in Eq. [55] of their work (22) as follows (converted to SI units):

$$R_o^2 \;\gg\; \frac{6D}{\delta\omega_s \cdot f_v^{2/3}} \quad , \quad \delta\omega_s \;=\; \frac{\gamma}{3}\cdot M_c \qquad [2]$$

where D is the diffusion coefficient, R_o is the mean magnetic compartment size and $\delta\omega_s$ is the resonant frequency offset at the external edge on the equator of the magnetic compartment, called the equatorial frequency offset. This SD regime limit definition is somewhat non-traditional as it requires a large diffusion time from one magnetic compartment location to another relative to the inverse frequency offset midway between particles. This differs from the traditional, and less restrictive, definition requiring diffusion time across the particle dimension, R_o, to be large relative to the inverse equatorial frequency offset, $\delta\omega_s^{-1}$.

Though well described by Yablonskiy and Haacke, the fundamental theory provided by Eqs. [1] and [2] has not been confirmed experimentally to date. The authors suggest application of their theory to quantifying free, uncompartmentalized iron-oxide nanoparticles, however, the static dephasing regime equations are likely to be more suited to the application of iron-oxide compartmentalized within cells. In this work, the validity of predictions for R_2' as well as the SD regime limit are tested for both compartmentalized and free iron-oxide suspensions.

Methods

THP-1 Cell Preparation

THP-1 cells were chosen to study intracellular iron signal effects as they can be prepared with a wide range of intracellular iron concentrations through phagocytosis of iron core SPM contrast agents. THP-1 cells are a human promonocytic cell line derived from acute monocytic leukemia (from the American Type Culture Collection). The cells were grown in 25-ml flasks with RPMI-1640 medium (Gibco) supplemented with 10,000 units/ml penicillin, 10 mg/ml streptomycin and 10% FBS at 37°C. 5×10^6 cells placed in 5 ml medium/dish were activated by adding 100 ng/ml of Phorbol 12-myristate 13-acetate for 5 days. After activation, non-adhered cells were removed through medium changes leaving approximately 4×10^6 cells/dish.

Two carboxydextran-coated magnetite nanoparticles were compared: SHU 555A (Schering AG, Berlin), a superparamagnetic iron oxide (SPIO) contrast agent with a mean particle size of about 60 nm; and a new ultrasmall superparamagnetic iron oxide (USPIO) contrast agent, SHU 555C (Schering AG, Berlin), having a mean particle size of about 20 nm. Iron loading was accomplished by adding either SPIO or USPIO contrast agent at one of 4 doses (0.05, 0.1, 0.2, 0.3 mgFe/ml) and 5 incubation times (6, 12, 24, 36, 48 hours). The dose group was incubated for 24 hours and the incubation time group using a dose of 0.1 mgFe/ml. After iron incubation, the adhered cells were detached by trypsinization (adding 0.05% trypsin for 3 minutes on ice) and washed in HBSS three times. The cell viability was then confirmed by the trypan-blue exclusion test and the number of cells were counted.

NMR samples for the dose and incubation time group were prepared with a cellular

concentration of 4 x 10^6 cells/ml. This corresponds to a cellular volume fraction of only 0.189%, given the reported THP-1 cell volume (23) of 473 $\pm$ 16 μm^3. Each 1 ml sample was placed within 5 mm NMR tubes and suspended in 2% w/w gelatin to prevent sedimentation. A cell density group, incubated for 24 hours at 0.1 mgFe/ml, was prepared by concentrating cells from multiple culture dishes after iron-oxide incubation. 1 ml NMR samples were prepared at 5 cellular densities (1, 2, 4, 8, 16 x 10^6 cells/ml). In total, 4 dose group samples, 4 unique incubation time samples, 5 cell density samples and a control sample, incubated for 24 hours without contrast agent present, were prepared using each contrast agent (see table 1).

Cellular Iron Quantification

Two properties of cellular iron loading were monitored: intracellular magnetization and iron mass per cell. Direct measurement of intracellular magnetization is important since this is the property that appears in theoretical treatments of susceptibility-induced NMR signal response. Magnetization was measured using a susceptometry technique, the Reilly-McConnell-Meisenheimer (RMM) method (24,25), modified in this work to use multi-echo imaging. Compared to measurements of spectral broadening, as employed by the original RMM method, this approach more accurately characterizes the susceptibility-induced field inhomogeneity pattern outside of a NMR tube oriented perpendicular to B_o. This NMR based susceptometry method permits non-destructive measurement of sample magnetization even in situations where extremely short relaxation times preclude conventional NMR relaxometry or spectroscopy.

Bulk magnetic susceptibility for any substance within a NMR tube can be estimated from the magnetic field inhomogeneity pattern established outside such a NMR tube oriented *orthogonal*

to $\mathbf{B}_o$. The solution to Maxwell's equation for the field offset produced external to co-axial cylindrical boundaries of differing susceptibility (glass walled NMR tube) is (24):

$$\Delta B(r) = \frac{B_o \cos 2\theta}{r^2}\left[-\frac{1}{2}\left(1+\frac{\chi_3}{3}\right)\right]\left[a_1^2(\chi_2-\chi_1) + a_2^2(\chi_3-\chi_2)\right] \qquad [3]$$

where χ_1, χ_2 and χ_3, are the bulk magnetic susceptibility within the NMR tube (desired), of the NMR glass and of the material external to the NMR tube (distilled water), respectively. a_1 and a_2 are the internal and external radii of the NMR tube (2.1, 2.5 mm), respectively. r is the radius to the field profile position of interest external to the NMR tube (i.e. $r = |\mathbf{r}|$ where $\mathbf{r}$ is the vector from tube origin to position of interest) and θ is the angle between $\mathbf{r}$ and $\mathbf{B}_o$. For samples with saturated magnetization, magnetization does not scale with static field and $\chi_1 B_o$ is replaced by *LMD*, the local magnetic dose (22). This is the case at normal MRI field strengths for superparamagnetic species like the two iron oxide nanoparticles used in this work (11,12,22).

The RMM apparatus consisted of a 5 mm outer diameter NMR tube concentrically placed, using teflon spacers, within a 15 mm inner diameter, 10-ml graduated cylinder. The graduated cylinder contained distilled water and the surfactant, Photo-Flo 200 (0.5%), to inhibit bubble formation. The apparatus was placed vertically within a 5 cm diameter solenoid RF coil in a 4 T Varian whole body scanner. The field inhomogeneity pattern was mapped by generating a field map from the phase evolution versus echo time in images acquired using a 2D multi-echo gradient echo sequence (128 x 128, 10 mm slice, 6 cm FOV, 8 ms echo spacing, 20 echoes). The field map was computed through a Fourier transform of the complex signal along the echo train for each pixel. The peak frequency for each pixel from the magnitude of the Fourier transform

9

defined the local field offset. A sample field map (0.05 mg/ml SPIO in gel) is shown in Fig. 1b. The corresponding magnitude image is shown in Fig. 1a. Phase wrap due to aliasing occurs for field offsets greater than the Nyquist frequency ($\pm 1/(2 \cdot esp)$ or ± 62.5 Hz).

Field map inhomogeneity external to the NMR tube was characterized by averaging 4 field profiles extending radially outward from the external edge of the NMR tube in each orthogonal direction. Figure 1c shows the 4 profiles corresponding to the field map of Fig. 1b. To correct for aliasing, each profile was unwrapped along the radial direction for frequency discontinuities greater than half the Nyquist frequency. Useful field profiles could thus be obtained as long as the *difference* in frequency offsets of adjacent pixels did not exceed the Nyquist frequency. Unwrapping discontinuities associated with aliasing for an entire image is challenging, so the inhomogeneity pattern was characterized using only 4 profiles to avoid these difficulties. To enhance SNR of the profiles and counter the effect of any global linear field variation across the image, the 4 profiles were averaged together (after appropriate polarity reversal of the two $\theta = 90°$ profiles).

This average profile was fit to the theoretical inhomogeneity pattern, shown in Eq. [3], to determine the susceptibility within the NMR tube. A two parameter constrained least squares fit of Eq. [3] was used. The average profile, along with the results of the fit, are shown in Fig. 1d. The two free parameters in the fit were χ_1, the sample susceptibility, and a baseline constant added to account for global resonance offset. The susceptibility of water (χ_3) and NMR tube glass (χ_2) were assumed to be -9.06 ppm and -9.77 ppm, respectively. χ_2 was measured using a water-filled tube, and fitting Eq. [3] for χ_2, with χ_1 and χ_3 constrained to equal the susceptibility

10

of water. Sample susceptibility was converted to mg/ml of Fe through calibration with known concentration reference samples of SPIO and USPIO, in the form of uniform suspensions of the nanoparticles in gelatin.

Iron concentrations for several samples were measured using atomic emission spectroscopy (AES). This method directly quantifies iron mass independent of valence. AES is also readily available in most hospital labs and hence represents a practical gold standard for validating the susceptometry method estimate of iron concentration. AES measurements were also used to verify that no cell lysis in cellular samples had occurred since lysis would cause the undesired release of iron-oxide into the extra-cellular gelatin. This was accomplished by gently heating the samples to 37°C (after all NMR measurements), separating the gelatin from the cells via centrifuging and performing AES on the isolated gelatin. On average for the 3 samples tested, only 6% of the iron in cellular samples was extracellular; this experiment confirmed that extracellular iron could be ignored in our analysis.

Relaxation Mechanism

The methods described in this section serve three purposes: to identify the dominant relaxation mechanism affecting NMR signal for iron-oxide loaded cells; to measure the relative sensitivity of different relaxation rates (R_1, R_2 and R_2^*) and to test the accuracy of static dephasing regime predictions in this case. Measurements were made at 1.89 T on a SMIS/Oxford 30 cm bore system and at 4 T on a Varian/Siemens whole body scanner.

Measurements were made at 1.89 T using a 2D hybrid relaxometry pulse sequence which simultaneously provided T_1 and T_2 relaxometry spectra (26). This approach produces both T_1 and

T_2 results in a scan time of approximately 5 minutes per sample (described in greater detail in Ref. 26). The experimental arrangement consisted of sample NMR tubes being placed within a 15 mm diameter solenoid RF coil orthogonal to the main field. Acquisition consisted of a non-selective CPMG train using a 90-180 pulse spacing, τ_{cpmg}, of 1.25 ms. The decay curve was sampled with 950 even echo times spanning 5 to 4750 ms. An inversion recovery pulse preceded the CPMG train with 30 different inversion times, TI, spanning 40 to 7000 ms. Processing consisted of a 2D non-negative least squares (NNLS) fit using 200 T_2 bins spanning 0-2000 ms and 35 T_1 bins spanning 0-3500 ms. The 2D spectra for all samples were dominated by a single peak and so the spectra were collapsed and reported as a single value of T_1 and T_2 corresponding to that peak. T_2^* was estimated using this same experimental arrangement at both 1.89 T and 4 T through measurement of the spectral linewidth from a pulse-acquire sequence. The R_2^* relaxation rate was estimated as $R_2^* = \pi \cdot FWHM$ where $FWHM$ is the full width at half maximum of the Lorentzian spectral line in Hz.

In order to further study the relaxation mechanism and test the static dephasing regime approximation, T_2 measurements were made at 4 T using a 2D multi-echo CPMG imaging pulse sequence (128 x 128, 10 mm slice, 6 cm FOV). Other than the pulse sequence, the experimental arrangement was identical to that described for NMR susceptometry in the previous section. Images were reconstructed for every echo of the CPMG train. Two different 90-180 CPMG pulse intervals, τ_{cpmg}, were used in separate acquisitions to sample 200 ms of the echo train (20 echoes with τ_{cpmg} = 5 ms and 10 echoes with τ_{cpmg} = 10 ms). The signal decay curve, generated from a region of interest within the NMR tube, was fit using 1D NNLS to produce a T_2 spectrum. Only one peak was found for all samples and the peak T_2 was used to report the sample T_2 value.

To ensure that the estimated T_2 was not biased by the different number of echo times sampling the signal decay curve for each τ_{cpmg}, the τ_{cpmg} = 5 ms signal decay curve was separately fit using either all echoes or only even echoes. No significant differences were observed.

Results

Cellular Iron Quantification

The susceptometry calibration curves for the SPIO and USPIO iron-oxide contrast agents are shown in Fig. 2. The slope of the calibration curves are 1319 ± 69 and 1360 ± 55 mG per mg/ml of Fe for SPIO and USPIO, respectively. All reported uncertainties refer to 95% confidence intervals throughout this section. The two SPM particle calibration slopes agree within uncertainty (p=0.05). For single magnetic domain, superparamagnetic iron-oxide particles having the same iron spin state, this should be the case (11,12). Since both SPM particles studied are preparations of similar 4.6 nM magnetite cores, differing only in number of cores per particle and overall particle size (27), agreement between the calibration slopes is not unexpected.

Table 1 summarizes the cellular iron uptake data for SPIO and USPIO. The results for the dose, incubation time and cellular density groups, as described in the methods section, are shown. AES iron concentration for 3 SPIO and 3 USPIO samples are shown in curly brackets for comparison with the susceptometry method and agree within uncertainty (p=0.05) with a 7% rms error. Figure 3 plots iron uptake in pgFe/cell for SPIO and USPIO. For each contrast agent, iron uptake for both dose and incubation time groups was plotted collectively versus the incubation time - dose product. As expected, higher doses and longer incubation times resulted in increased

uptake. This uptake was linear when plotted against either dose or incubation time independently (not shown) with all curves having correlation coefficients greater than 0.97.

Assuming this linearity remains valid for a distribution of doses and incubation times around the reference dose and incubation time (0.1 mgFe/ml and 24 hours), an *uptake efficiency* can be defined about this reference. In Fig. 3, uptake efficiency is reflected by the slope of iron uptake (pgFe/cell) versus the product of incubation time and dose, using data from both dose and incubation time groups. The correlation coefficient was 0.97 and 0.98 for the SPIO and USPIO uptake curves, respectively, supporting the legitimacy of a linear fit. The uptake efficiencies for SPIO and USPIO were determined to be 3.06 ± 0.40 and 0.80 ± 0.08 pgFe/cell per hour•dose, respectively. There was no evidence of iron uptake saturation, or a reduced rate of iron uptake after time, during phagocytosis for THP-1 cells over the range of doses and incubation times studied. This is perhaps not surprising considering that phagocytosis is a concentration mediated process that eventually results in cell death rather than saturation. Our cell viability tests indicated that even at the highest uptake, cell death had not occurred to any significant extent.

Relaxation Mechanism

Figure 4 shows the relative sensitivity of different NMR relaxation rates at 1.89 T to the presence of iron-oxide compartmentalized within THP-1 cells. The relaxation rates are plotted for the constant cellular density SPIO and USPIO groups. A log-log plot was used because of variation over 2 orders of magnitude in the R_1, R_2 and R_2^* relaxation rates. Table 2 lists the relaxivity of each NMR time constant obtained from linear regression for both SPIO and USPIO in cells. In each of the R_1, R_2 and R_2^* cases, relaxivities for SPIO and USPIO are similar, agreeing

to within 40%, although different at the 95% confidence level. On average for each iron-oxide particle, R_2^* is 70 times greater than R_2 and 3100 times greater than R_1, for SPM loaded cells. As mentioned in the Theory section, this observation is consistent with cellular scale bulk magnetic susceptibility effects violating the extreme motional narrowing assumption implicit in quantum dipolar relaxation theory (13,15). However, the question of whether the cellular magnetic moment is large enough to satisfy conditions of SD regime theory, described by Yablonskiy and Haacke (22), still remains.

Figure 5 demonstrates the impact of iron-oxide compartmentalization within cells on R_2^* relaxivity. The R_2^* relaxation rate curves, measured at 4 T, are plotted for SPIO and USPIO in gel suspensions as well as compartmentalized within cells. All data from the dose, incubation time and cellular density groups are included. It is important to recall that each value of *LMD* corresponds to a specific iron-oxide concentration so that differences between curves reflect differences due to the microscopic distribution, not to the concentration of iron-oxide. The static dephasing regime theoretical prediction for R_2', described in Eq. [1], is also plotted for comparison. The intercept for this curve is the R_2^* relaxation rate measured from the control cell suspension that was not exposed to iron-oxide nanoparticles. Although R_2^* is given by the addition of R_2' and R_2, the R_2 component was neglected since table 2 indicates that R_2 is at least 70 times less than R_2^* and hence R_2'. The theory curve represents the maximum relaxation rate possible as described by the static dephasing regime theory.

The R_2^* relaxation rates per unit LMD ("relaxivity") obtained from the linear regression slopes of each curve are listed in table 3. The relaxivities for SPIO at 4 T and USPIO at 1.89 T

agree with SD regime theory within the 95% confidence interval, while the relaxivities for SPIO at 1.89 T and USPIO at 4 T are 40% higher. Outer sphere dipolar field SD regime theory predicts a relaxivity of 10.78 s^{-1} mG^{-1} (Eq. [1]). No field strength dependence in R_2^* relaxivity was observed: these relaxivities averaged across the two iron-oxide agents compartmentalized within cells were 13.5 ± 2.3 and 12.8 ± 1.6 s^{-1} mG^{-1} at 1.89 T and 4 T, respectively. This is expected for iron-oxide contrast agents since saturation of SPM magnetization occurs for any field strength greater than 1 T (11,12,22). Similarly, no dependence on SPM particle size was observed: the R_2^* relaxivities averaged over each field strength were 13.3 ± 1.6 and 12.9 ± 2.3 s^{-1} mG^{-1} for SPIO and USPIO respectively. This too is expected if cellular bulk magnetic susceptibility satisfies conditions of the static dephasing regime and is the dominant mechanism of relaxation.

The R_2^* relaxivities of both SPIO and USPIO suspended in gel were significantly less than those of the iron-oxide agents compartmentalized within cells, being a factor of 3 and 8 less than SD regime theory predictions, respectively. The reduction in R_2^* for free, uniformly distributed SPM particles is expected since individual iron-oxide cores do not have enough iron to produce outer sphere inhomogeneity patterns which are strong enough to prevent the rate-reducing effects of motional averaging. Iron-oxide cores have a mass of only 1.92 x 10^{-7} pg of iron. This is derived using the known density of iron-oxide (3.76 gFe/cm^3) (28) and the size of the iron-oxide core (4.6 nM) (4,27). In the appendix, the SD regime definition is reformulated in terms of *LMD*, in mG, and iron mass per compartment (m_c), in pico-grams. The result is Eq. [A7], shown here:

$$m_c \gg \frac{0.216}{\sqrt{LMD}}$$

$$LMD \gg \frac{0.0465}{m_c^2} \qquad\qquad [4]$$

For single-core iron-oxide particles in uniform suspension, using 1.92×10^{-7} pg as the mass of iron per iron-oxide core, accurate SD regime predictions are only expected for $LMD \gg 10^{12}$ mG. From the calibration shown in Fig. 2, this corresponds to an iron concentration greater than 7×10^8 mg/ml, which is much larger than can be obtained in practice. This SD regime limit describes the case of SHU 555C, the USPIO studied, as it is a monocrystaline iron-oxide nanoparticle (MION), having only one iron-oxide core per particle. The SPIO studied, SHU 555A, is a polycrystaline iron-oxide nanoparticle (PION) having multiple iron-oxide cores per particle. Since SPIO has a greater mass of iron per particle, SPIO in uniform suspension has a larger R_2^* relaxivity as it more closely approaches, though does not yet reach, the SD regime limit for practical LMD values, as expressed by Eq. [4]. The agreement of the relaxivity measurements for the cellular suspensions with the predictions of SD regime theory is striking, though upon reflection not unexpected, since table 1 indicates that the smallest mass of iron within any cell used was 0.7 pg. In this case, SD regime predictions are valid for $LMD \gg 0.1$ mG. All iron-oxide loaded cell samples in our experiments had measured LMD values well above this range. *We conclude from these experiments the remarkable fact that cellularly compartmentalized iron-oxide, at any reasonable loading level, leads to R_2^* relaxivity that is both maximized and can be easily and accurately predicted from SD theory, whereas free iron-oxide nanoparticles are neither large enough nor dense enough to approach the SD relaxivity limit.*

To further investigate the reliability of static dephasing regime predictions for cellularly

compartmentalized iron-oxide, the CPMG 90-180 pulse interval (τ_{cpmg}) dependence of R_2 was explored at 4 T for the constant cellular density groups. Figure 6 shows the R_2 versus *LMD* curves for SPIO and USPIO acquired using a τ_{cpmg} of 5 ms and 10 ms. As detailed in the Theory section, no explicit analytic theory for large magnetic perturbers exists to predict R_2 dependence, so the solid lines are merely second order polynomial fits to the data to guide the eye. There are two clear observations: R_2 increases with *LMD* for all curves and R_2 is greater for the τ_{cpmg} = 10 ms than the τ_{cpmg} = 5 ms curve. There are two possible explanations for the observed increase in R_2 with *LMD*: intracellular diffusion through outer sphere dipolar field inhomogeneities of iron-oxide cores, as best described by quantum dipolar relaxation theory; or extracellular diffusion through dipolar field inhomogeneities produced by cellular BMS differences. The second observation of increased R_2 with τ_{cpmg} indicates that BMS effects contribute, at least in part, to the R_2 relaxation, and that some deviation from predictions of the SD regime are observable. However, this non-zero BMS contribution to R_2 is slight, being at least 70 times less than R_2^*, so deviation from the purely static dephasing regime for cellularly compartmentalized iron-oxide is minimal.

R_2 sensitivity to compartmentalized iron-oxide concentration was further explored by varying concentration through changes in cell density versus iron content per cell. Figure 7 plots R_2 versus *LMD* for the variable cell loading samples (dose and incubation time groups) and the variable cell density samples (cell density group) for both SPIO and USPIO at 4 T with τ_{cpmg} = 5ms. Again, *LMD* is directly proportional to iron concentration and second order polynomial fits are included merely to guide the eye. R_2 is clearly more sensitive to increased iron concentration for the variable cell density group than for the variable cell loading group. Two properties

explain this result: R_2 sensitivity is a measure of deviation from the predictions of SD regime theory; and SD regime predictions become more accurate as the mass of iron per cell increases (see Eq. [4]). For the variable cell loading group, increasing iron concentration by increasing iron mass per cell causes the samples with more iron per cell to better approximate the SD regime and hence, to have reduced R_2 relative to the variable cell density group. This argument also provides an explanation for the sub-linear response of R_2 to *LMD* for the variable cell loading group.

Discussion

Cellular Iron Uptake

Before studying the relative sensitivity and specificity of various NMR relaxation parameters (R_1, R_2 and R_2^*) to the presence of iron-oxide in cells, a means of assessing the mass of iron ingested through phagocytosis was necessary. The RMM method of MR susceptometry (24,25), modified by us to directly image the field inhomogeneity pattern, met this requirement. In addition, MR susceptometry served to measure sample magnetization and thus allowed a direct assessment of SD regime theoretical predictions. Quantifying iron-oxide uptake during phagocytosis confirmed that the magnetic label does not decay over the 48 hour iron-oxide incubation time studied (29). Preservation of the magnetic label over a number of days was confirmed by the agreement between AES and susceptometry estimates of iron mass per cell. Breakdown of the iron-oxide core following phagocytosis would have destroyed the SPM core magnetic moment causing sample susceptibility to drop dramatically (29). Preservation of the SPM magnetic moment after phagocytosis is important for achieving optimal sensitivity and quantifiability of macrophage cell number/density *in vivo*.

The uptake of iron-oxide was found to be linear with dose and incubation time to very large loading levels, permitting the definition of an uptake efficiency. Linearity with incubation time was previously demonstrated by Pratten and Lloyd (30) using radioactively labeled polystyrene beads with peritoneal macrophages. Uptake linearity is confirmed in this work for dose variation and for the more applicable SPM particles. Uptake of iron-oxide was nearly four times more efficient with the larger SPIO particles than with USPIO. This is consistent with the result of Pratten and Lloyd (30) that described an increased phagocytic contribution to particle volume uptake with increasing size of polystyrene beads. Since the iron density for the two SPM particles studied differ, a quantitative comparison of the relative uptake rates for these particle sizes with the work of Pratten and Lloyd is not possible. However, more important for targeted imaging applications, the mass of iron ingested within cells is predictable, with a unique uptake efficiency being described for every nanoparticle and phagocytic cell type.

Being able to quantify relative uptake efficiency for different SPM particles has implications both for *in vitro* and *in vivo* loading methods. *In vitro* loading methods, used for cell trafficking (8), require fast, efficient loading of iron-oxide into cells prior to re-injection. Quantifying uptake of different iron-oxide particle preparations may help clarify the most efficient particle for this purpose. Knowledge of the iron-oxide mass per cell is important for estimates of cellular detection threshold. *In vivo* loading methods, where SPM particles are injected directly into the bloodstream, may also benefit from quantification of iron-oxide uptake. There are many factors affecting the efficiency of SPM uptake by targeted cells (7). These include RES clearance of SPM particles from the bloodstream, tissue perfusion, target cell uptake efficiency, SPM particle breakdown and SPM particle clearance from tissue via the lymphatic system. Particle clearance

20

and tissue perfusion rates can be measured by other methods. Therefore, measurement of target cell uptake efficiency may provide the critical missing information for estimating *in vivo* rates of particle uptake by targeted cell populations.

Sensitivity and Quantification

The NMR parameter (R_1, R_2 or R_2^*) which was most sensitive to the presence of iron-oxide within cells was explored. As indicated in table 2, R_2^* relaxivity was 70 times greater than R_2 and 3100 times greater than R_1, for iron-oxide compartmentalized within cells. The main effect of compartmentalization was to greatly increase the relative R_2^* sensitivity, compared to the uniformly distributed iron-oxide case, where R_2^* and R_2 are of the same order (4,14). However, the relative sensitivity of image signal intensity to the presence of iron-oxide is not determined solely by relaxivity. The relative contrast to noise (CNR) of T_1, T_2 or T_2^* weighted acquisitions, with and without iron-oxide present, is derived from iron-oxide-induced relaxation enhancement, as well as the baseline tissue relaxation rates measured prior to iron-oxide injection (15). While baseline tissue relaxation rates are different for every tissue and field strength, R_2^* is typically no more than 1 order of magnitude greater than R_2 and 2 orders of magnitude greater than R_1. Since the iron-oxide-induced relaxation enhancement for R_2^* was measured to be approximately 2 and 3 orders of magnitude greater than for R_2 and R_1, respectively, R_2^* weighted acquisitions are potentially the most sensitive to the presence of cellularly compartmentalized iron-oxide particles. Calculations of CNR for R_2^* weighted acquisitions are beyond the scope of this work, but are possible using predictions of SD regime theory, confirmed for SPM loaded cells here, and from knowledge of baseline tissue R_2^* sources.

21

A new approach to quantifying the concentration of iron-oxide compartmentalized within cells is another outcome of this work. We achieved this by examining which exchange regime equations were most valid for describing outer sphere dipolar field relaxation in the case of cellular iron compartmentalization. The quantum solution, which relies on the extreme motional narrowing approximation, has previously been shown to adequately describe the R_1 and R_2 relaxivity of uniformly distributed SPM particles (12,13,31). Since this theory predicts R_2 and R_2^* equivalence, the observation that R_2^* is as much as 70 times larger than R_2 relaxivity for cellularly compartmentalized SPM clearly invalidates predictions of the quantum solution in this case. This demonstration of homogeneous broadening on the NMR timescale, and the τ_{cpmg} dependence of R_2, are consistent with cellular scale BMS differences being the mechanism of R_2 sensitivity to cellularly compartmentalized iron-oxide. The magnetic moment of the entire cell taken as a single magnetic compartment produces a large enough outer sphere dipolar field to violate the extreme motional narrowing assumption implicit in the quantum theory.

Though much smaller than R_2^*, and without a clear theoretical framework to predict relaxation rate for cellularly compartmentalized iron-oxide, R_2 does show sensitivity to iron concentration and so is a candidate for empirical quantification of iron concentration. As indicated in Fig. 7, R_2 demonstrates iron-oxide sensitivity, which is different depending on whether iron mass per cell or cell concentration is varied to alter sample iron-oxide concentration. Concentrating more SPM into fewer cells produces a better approximation to the SD regime and hence, a reduction in R_2. Therefore, R_2 is sensitive to both concentration and distribution of SPM, which greatly complicates its use for quantifying iron-oxide concentration.

The SD regime predictions for R_2' agreed, within uncertainty, with measurements for the cellularly compartmentalized SPM in two of four cases (SPIO at 4 T and USPIO at 1.89 T), while measured R_2' was significantly higher than SD regime theory for the other cases (USPIO at 4 T and SPIO at 1.89 T). Overall, we observe a 21% elevation in R_2' relative to SD regime theory for a volume fraction of 0.189%. Brooks et al. (31) have noted a 33% increase in R_2^* with Monte Carlo simulations compared to SD regime theory predictions. The authors postulate that the large perturber volume fraction in their simulations (0.5%) violated the dilute perturber approximation implicit in SD regime theory. In this case, field profile overlap between different perturbers eliminates signal from regions furthest from the perturber, where field gradients are the lowest, leading to an increased relaxation rate. Monte Carlo simulations with very small volume fraction (2×10^{-6}), by Muller et al. (17), produce R_2' values that are elevated by 10%, relative to theoretical values, but which agree within uncertainty (as noted by Yablonskiy and Haacke (22)). For most *in vivo* applications, the volume fraction of cells containing iron-oxide will likely be small enough to satisfy the dilute perturber requirement; hence, we expect that SD regime theory will be more closely approximated *in vivo* than in our more artificial cell culture conditions.

As detailed in the results section, all iron-oxide loaded cell samples tested met the SD regime requirement for mass of iron per compartment, while the uniformly distributed SPM in gel samples did not. As a result, uniformly distributed SPM samples had R_2' relaxivities 3 and 8 times less than SD regime theory for SPIO and USPIO, respectively. Although samples which clearly satisfied or clearly failed the static dephasing regime condition were measured in this work, the transition region defining onset of the SD regime, given in Eq. [2], was not carefully probed. However, Monte Carlo simulations by Muller et al. (17) do support the SD regime

equation defined by Yablonskiy and Haacke (22). Equation [2] defines the SD regime as $R_o >$ 0.19 μm, while the conventional definition, given as $R_o^2 >> 6D/\delta\omega_s$, defines the SD regime as R_o > 0.02 μm (calculations using the parameters: $f_v = 2 \times 10^{-6}$, $\delta\omega_s = 3.4 \times 10^7$ s^{-1} and $D = 2.5 \times 10^{-5}$ cm^2 s^{-1}). Figure 1 in the work of Muller et al. supports the prediction of Eq. [2] since R_2^* has clearly reached the peak value for $R_o > 0.19$ μm, while R_2^* is only 60% of peak for $R_o > 0.02$ μm in that work.

For cellularly compartmentalized SPM particles, R_2' is potentially the most sensitive and the most quantifiable NMR parameter. However, it is necessary that the mass of iron per cell be sufficient to guarantee static dephasing regime predictions in order to relate R_2' with iron-oxide concentration. Assuming, for the sake of argument, that the presence of SPM particles must enhance R_2' by at least 100 s^{-1} to be well-distinguished from background sources, *LMD* and *[Fe]* must exceed 9.3 mG and 6.9 μg/ml, respectively. This is derived from Eq. [1], and the calibration curve in Fig. 2, respectively. For this minimally detectable R_2', the mass of iron per particle, as calculated using Eq. [4], must exceed 0.07 pg per cell to guarantee SD regime predictions. Based on loading levels that we and others have achieved (4), we expect that this condition will be met by most cell trafficking studies (which use *in vitro* loaded cells) and may be met for studies of inflammatory models using injection of free SPM particles with subsequent *in vivo* cell uptake.

Conclusions

The relaxation properties of SPM particles that are compartmentalized within cells were studied and found to satisfy predictions of static dephasing regime theory under conditions

typical for many *in vivo* applications. The required conditions are that the mass of iron per cell exceed a known threshold to ensure the validity of SD regime predictions. To test SD regime theory, it was necessary to develop methods measuring cellular iron-oxide uptake and sample susceptibility. An imaging version of the RMM susceptometry technique was developed to meet these requirements. In addition, the linearity of phagocytic uptake of iron-oxide with dose and incubation time was demonstrated for THP-1 cells, permitting the definition of an uptake efficiency, unique for every cell and particle type.

Under conditions satisfying the SD regime, the greatest sensitivity to cellularly compartmentalized iron-oxide was observed with R_2^*, rather than R_2 or R_I. This differs from the case of uniformly distributed SPM particles, where relative sensitivity between parameters is more similar. In addition, R_2' was best for quantifying iron-oxide concentration. This is because analytical theories for R_2 and R_I are lacking when SPM particles are compartmentalized within cells, whereas SD regime theory correlating SPM-particle-induced R_2' enhancement with iron-oxide concentration was proven to be accurate. R_2' showed sensitivity to iron-oxide concentration alone, rather than both concentration and mass of iron per cell, as was observed with R_2. The non-unique dependence of R_2 on mass of iron per cell greatly complicates its use for quantifying cellularly compartmentalized iron-oxide concentration. For in vivo conditions, R_2' may yet prove to be both the most sensitive and the most quantifiable parameter for estimating iron-oxide concentration.

Appendix

The static dephasing regime definition, formulated by Yablonskiy and Haacke (Eq. [2]), can

be rewritten as:

$$f_v \;\gg\; \left[\frac{18 D f_v}{R_o^2 \, \gamma \, LMD} \right]^3 \qquad\qquad\qquad \text{[A1]}$$

where definitions listed in the introduction for $\delta\omega_s$ ($\delta\omega_s \equiv \gamma M_c/3$), and LMD (LMD$\equiv f_v M_c$), in SI units, have been used. Solving for f_v, one obtains the expression:

$$f_v \;\ll\; \left[\frac{\gamma \, LMD \, R_o^2}{18 D} \right]^{3/2} \qquad\qquad\qquad \text{[A2]}$$

The inequality involving f_v has reversed from the initial expression reported in Eq. [A1]. This form is more intuitive since, for a given local magnetic dose (iron concentration), compartmentalization of magnetic particles to less than some maximum fractional volume, f_v, is necessary for accurate static dephasing regime predictions.

An expression that describes the static dephasing regime in terms of the required mass of iron per compartment is desired. An expression calibrating magnetic dose, LMD, with iron concentration is necessary to achieve this:

$$LMD \;=\; K_{Fe} \, n_c \, m_c \qquad\qquad\qquad \text{[A3]}$$

where n_c is the compartment density, m_c is the mass of iron within each compartment and K_{Fe} is a calibration coefficient relating iron concentration to magnetic dose. Using the fractional volume definition, $f_v \equiv n_c V_c$, where V_c is the compartment volume, and Eq. [A3], Eq. [A2] becomes:

$$n_c \, \tfrac{4}{3}\pi R_o^3 \quad \ll \quad \left[\frac{\gamma \, K_{Fe} \, n_c \, m_c \, R_o^2}{18 D} \right]^{\!3/2} \qquad \text{[A4]}$$

Canceling common powers of n_c and R_o and squaring both sides, the equation simplifies to:

$$\left(\tfrac{4}{3}\pi\right)^2 \quad \ll \quad \left[\frac{\gamma \, K_{Fe} \, m_c}{18 D} \right]^3 n_c \;=\; \left[\frac{\gamma}{18 D} \right]^3 \left[K_{Fe} \, m_c \right]^2 LMD \qquad \text{[A5]}$$

where LMD has been reinserted using Eq. [A3]. Finally, the static dephasing regime equation can be evaluated for either m_c or LMD as follows:

$$m_c \quad \gg \quad \left[\frac{4\pi}{3 K_{Fe}} \right]\left[\frac{18 D}{\gamma} \right]^{3/2} LMD^{-1/2}$$

$$LMD \quad \gg \quad \left[\frac{4\pi}{3 K_{Fe} \, m_c} \right]^2 \left[\frac{18 D}{\gamma} \right]^3 \qquad \text{[A6]}$$

The SD regime predictions will only be reliable if the mass of iron per compartment is great enough to satisfy Eq. [A6] for the minimum LMD in the range being measured. Conversely, for a given m_c, measurements are reliable only when LMD exceeds that in Eq. [A6].

The expressions in Eq. [A6] can be further simplified if the calibration coefficient between magnetic dose and iron concentration, K_{Fe}, is known. In Fig. 2, this calibration was shown to agree within uncertainty for the two iron-oxide particles studied, with a mean value of $K_{Fe} = 1.340 \times 10^{-3} \, mG/(pg/mm^3)$. Using this value for K_{Fe}, the self-diffusion coefficient for free water ($D = 2.5 \times 10^{-3} \, mm^2 \, s^{-1}$) and the proton gyromagnetic ratio ($\gamma = 26.752 \, rad \, mG^{-1} \, s^{-1}$), Eq. [A6] can be simplified as follows:

$$m_c \gg \frac{0.216}{\sqrt{LMD}}$$

$$LMD \gg \frac{0.0465}{m_c^2} \qquad \text{[A7]}$$

where the mass of iron within a compartment, m_c, is in pico-grams and the local magnetic dose, LMD, is in milli-gauss.

Acknowledgements

References

1. Bruck W, Sommermeier N, Bergmann M, Zettl U, Goebel HH, Kretzschmar HA, Lassmann H, Macrophages in multiple sclerosis, Immunobiology 1996;195:588-600.

2. Bruck W, Porada P, Poser S, Rieckmann P, Hanefeld F, Kretzschmar HA, Lassmann H, Monocyte/macrophage differentiation in early multiple sclerosis lesions, Annals of Neurology 1995;38:788-96.

3. Li H, Newcombe J, Groome NP, Cuzner ML, Characterization and distribution of phagocytic macrophages in multiple sclerosis plaques, Neuropathology & Applied Neurobiology 1993;19:214-23.

4. Weissleder R, Cheng HC, Bogdanova A, Bogdanov A Jr, Magnetically labeled cells can be detected by MR imaging, Journal of Magnetic Resonance Imaging 1997;7:258-63.

5. Dousset V, Delalande C, Ballarino L, Quesson B, Seilhan D, Coussemacq M, Thiaudiere E, Brochet B, Canioni P, Caille JM, In vivo macrophage activity imaging in the central nervous system detected by magnetic resonance, Magnetic Resonance in Medicine 1999;41:329-33.

6. Moore A, Marecos E, Bogdanov A Jr, Weissleder R, Tumoral distribution of long-circulating

dextran-coated iron oxide nanoparticles in a rodent model, Radiology 2000;214:568-74.

7. Suwa T, Ozawa S, Ueda M, Ando N, Kitajima M, Magnetic resonance imaging of esophageal squamous cell carcinoma using magnetite particles coated with anti-epidermal growth factor receptor antibody, International Journal of Cancer 1998;75:626-34.

8. Krieg FM, Andres RY, Winterhalter KH, Superparamagnetically labelled neutrophils as potential abscess-specific contrast agent for MRI, Magnetic Resonance Imaging 1995;13:393-400.

9. Schmitz SA, Coupland SE, Gust R, Winterhalter S, Wagner S, Kresse M, Semmler W, Wolf KJ, Superparamagnetic iron oxide-enhanced MRI of atherosclerotic plaques in Watanabe hereditable hyperlipidemic rabbits, Investigative Radiology 2000;35:460-71.

10. Furman-Haran E, Margalit R, Grobgeld D, Degani H, High resolution MRI of MCF7 human breast tumors: complemented use of iron oxide microspheres and Gd-DTPA, Journal of Magnetic Resonance Imaging 1998;8:634-41.

11. Fahlvik AK, Klaveness J, Stark DD, Iron oxides as MR imaging contrast agents, Journal of Magnetic Resonance Imaging 1993;3:187-94.

12. Bulte JW, Brooks RA, Moskowitz BM, Bryant LH Jr, Frank JA, Relaxometry and magnetometry of the MR contrast agent MION-46L, Magnetic Resonance in Medicine 1999;42:379-84.

13. Koenig SH, Kellar KE, Theory of 1/T1 and 1/T2 NMRD profiles of solutions of magnetic nanoparticles, Magnetic Resonance in Medicine 1995;34:227-33.

14. Majumdar S, Zoghbi SS, Gore JC, The influence of pulse sequence on the relaxation effects of superparamagnetic iron oxide contrast agents, Magnetic Resonance in Medicine 1989;10:289-301.

15. Koenig SH, Solvent relaxation by uniformly magnetized solute spheres. The classical-quantal connection, Investigative Radiology 1998;33:822-7.

16. Weisskoff RM, Zuo CS, Boxerman JL, Rosen BR, Microscopic susceptibility variation and transverse relaxation: theory and experiment, Magnetic Resonance in Medicine 1994;31:601-10.

17. Muller RN, Gillis P, Moiny F, Roch A, Transverse relaxivity of particulate MRI contrast media: from theories to experiments, Magnetic Resonance in Medicine 1991;22:178-82.

18. Hardy PA, Henkelman RM, Transverse relaxation rate enhancement caused by magnetic particulates, Magnetic Resonance Imaging 1989;7:265-75.

19. Fisel CR, Ackerman JL, Buxton RB, Garrido L, Belliveau JW, Rosen BR, Brady TJ, MR contrast due to microscopically heterogeneous magnetic susceptibility: numerical simulations

and applications to cerebral physiology, Magnetic Resonance in Medicine 1991;17:336-47.

20. Majumdar S, Gore JC, Studies of diffusion in random fields produced by variations in susceptibility, Journal of Magnetic Resonance 1998;78:41-55.

21. Brown R, Distribution of fields from randomly placed dipoles: free-precession signal decay as result of magnetic grains, Physical Review 1961;121:1379-82.

22. Yablonskiy DA, Haacke EM, Theory of NMR signal behavior in magnetically inhomogeneous tissues: the static dephasing regime, Magnetic Resonance in Medicine 1994;32:749-63.

23. Cohn RG, Mirkovich A, Dunlap B, Burton P, Chiu SH, Eugui E, Caulfield JP, Mycophenolic acid increases apoptosis, lysosomes and lipid droplets in human lymphoid and monocytic cell lines, Transplantation 1999;68:411-8.

24. Chu SC, Xu Y, Balschi JA, Springer CS, Bulk magnetic susceptibility shifts in NMR studies of compartmentalized samples: use of paramagnetic reagents, Magnetic Resonance in Medicine 1990;13:239-62.

25. Reilly CA, McConnell HM, Meisenheimer RG, Nuclear magnetic resonance spectra of annular samples, Physical Review 1955;98:264.

26. Saab G, Thompson RT, Marsh GD, Picot PA, Moran GR, Two-dimensional time correlation relaxometry of skeletal muscle *in vivo* at 3 Tesla, Magnetic Resonance in Medicine, in press.

27. Weinmann HJ, private communication.

28. Sjogren CE, Johansson C, Naevestad A, Sontum PC, Briley-Saebo K, Fahlvik AK, Crystal size and properties of superparamagnetic iron oxide (SPIO) particles, Magnetic Resonance Imaging 1997;15:55-67.

29. Weissleder R, Stark DD, Engelstad BL, Bacon BR, Compton CC, White DL, Jacobs P, Lewis J, Superparamagnetic iron oxide: pharmacokinetics and toxicity, AJR. American Journal of Roentgenology 1989;152:167-73.

30. Pratten MK, Lloyd JB, Pinocytosis and phagocytosis: the effect of size of a particulate substrate on its mode of capture by rat peritoneal macrophages cultured in vitro, Biochimica et Biophysica Acta 1986;881:307-13.

31. Brooks RA, Moiny F, Gillis P, On T2-shortening by weakly magnetized particles: The chemical exchange model, Magnetic Resonance in Medicine 2001;45:1014-20.

Table 1: Summary of Cellular Iron Uptake Data

	SPIO in Cells			USPIO in Cells		
	LMD [a] (mG)	$[Fe]_{sample}$ [b] (μg/ml)	mass/cell [d] (pg of Fe)	LMD [a] (mG)	$[Fe]_{sample}$ [b] (μg/ml)	mass/cell [d] (pg of Fe)
(mg/ml)	Dose Group (24 hours, 4 million cells/ml)					
0.05	31.8	24.1	6.0	7.4	5.4	1.4
0.1	46.4	35.2	8.8	15.5	11.4	2.9
0.2	99.5	75.4	18.9	23.9	17.6	4.4
0.3	129.2	98.0	24.5	33.4	24.6	6.1
(hours)	Incubation Time Group (0.1 mg/ml, 4 million cells/ml)					
6	19.1	14.5	3.6	4.1	3.0	0.7
12	35.8	27.2	6.8	6.7	4.9	1.2
24	46.4	35.2	8.8	15.5	11.4	2.9
36	65.6	49.7	12.4	18.2	13.4	3.3
48	76.2	57.7	14.4	22.7	16.7	4.2
(million cells/ml)	Cell Density Group (0.1 mg/ml, 24 hours)					
1	13.3	10.1 {9.5} [c]	10.1	6.8	5.0 {4.0} [c]	5.0
2	24.5	18.6	9.3	10.0	7.4	3.7
4	46.4	35.2 {46.4}	8.8	18.3	13.5 {16.7}	3.4
8	88.4	67.0	8.4	28.3	20.8	2.6
16	167.0	126.7 {170.9}	7.9	69.5	51.1 {52.7}	3.2

[a]Local Magnetic Dose of cellular samples obtained using susceptometry at 4 T. Reported LMD is given relative to the reference cellular sample that was not exposed to iron-oxide.
[b]Sample iron concentration determined from LMD and calibration in Fig. 2.
[c]Sample iron concentration determined from AES in brackets.
[d]Mass of iron per cell determined from sample iron concentration and mean cell count.

Table 2: Relative Relaxivities at 1.89 T of Iron-Oxide Loaded Cells

Relaxivities at 1.89 T	SPIO (s^{-1} mG^{-1})	USPIO (s^{-1} mG^{-1})
R_1/LMD	0.0036 ± 0.0005	0.0051 ± 0.0015
R_2/LMD	0.218 ± 0.018	0.165 ± 0.023
R_2^*/LMD	15.6 ± 1.0	11.3 ± 2.1

Table 3: Effect of Compartmentalization on R_2^* Relaxivity

Compartment Type	R_2^* at 1.89 T (s^{-1} mG^{-1})	R_2^* at 4 T (s^{-1} mG^{-1})
SD Theory [a]	10.78	10.78
SPIO in Cells	15.6 ± 1.0	11.0 ± 1.3
USPIO in Cells	11.3 ± 2.1	14.5 ± 1.0
SPIO in Gel	----	3.8 ± 0.3
USPIO in Gel	----	1.4 ± 0.2

[a]Outer Sphere Static Dephasing Regime prediction from Eq. [1].

Figure Captions:

Figure 1: Demonstration of susceptometry method. (a) magnitude image and (b) field map obtained from axial slice through NMR tube concentrically located within water filled graduated cylinder. 4 radial field map profiles were selected (heavy bar), plotted individually (c), averaged together (triangles in d), and fit to Eq. [3] (solid line in d) to obtain each sample susceptibility (χ_i). The estimate for χ_i was -7.61 ± 0.02 ppm for the 0.05 mg/ml SPIO suspension shown.

Figure 2: Calibration curves relating SPM magnetization to iron concentration for SPIO (triangles) and USPIO (circles) suspensions. The LMD is defined relative to pure gelatin. Linear regression of the SPIO (solid line) and USPIO (dashed line) data produced calibration slopes of 1319 ± 69 and 1360 ± 55 mG per mg/ml, respectively.

Figure 3: Cellular iron uptake curves indicating the mass of iron per cell which is taken up per unit dose and incubation time. Data for SPIO (triangles) and USPIO (circles) are shown for both the dose groups (solid symbols) and incubation time groups (open symbols). The slope from linear regression of the SPIO (solid line) and USPIO (dashed line) data defined the uptake efficiency as 3.06 ± 0.40 and 0.80 ± 0.08 pg of iron per mg/ml•hrs respectively.

Figure 4: Relaxivity curves indicating the R_1 (squares), R_2 (circles) and R_2^* (triangles) relaxation rates as a function of *LMD* for cellularly compartmentalized SPM samples. Data for SPIO (solid symbols) and USPIO (open symbols) are shown for the combined dose and incubation time groups. The slope from linear regression of the SPIO (solid line) and USPIO (dashed line) data defined the relaxivities as listed in table 2. Note that R_2^* is nearly 2 orders of magnitude greater

than R_2 for cellularly compartmentalized SPM.

Figure 5: R_2^* relaxivity curves at 4 T demonstrating the effect of SPM compartmentalization. The R_2^* relaxation rate for SPIO (triangles) and USPIO (circles) are shown as a function of LMD for cellularly compartmentalized SPM samples (solid symbols) and free SPM suspensions in gel (open symbols). The slope from linear regression for the SPIO (thin solid lines) and USPIO (thin dashed lines) data determined the relaxivities as listed in table 3. Note that R_2^* increases dramatically when SPM is compartmentalized within cells and agrees well with predictions of SD regime theory (thick solid line).

Figure 6: Demonstration of diffusion effects on R_2 relaxation rate sensitivity. The R_2 relaxation rate for cellularly compartmentalized SPIO (triangles) and USPIO (circles) are shown as a function of LMD for CPMG acquisitions having τ_{cpmg} equal to 5 ms (solid symbols) or 10 ms (open symbols). The curves for SPIO (solid line) and USPIO (dashed line) have no theoretical basis and serve only to guide the eye. Note that R_2 increases slightly with τ_{cpmg} indicating some deviation from the static dephasing condition.

Figure 7: R_2 relaxation rate curves demonstrating the effect of SPM compartmentalization. The R_2 relaxation rate for SPIO (triangles) and USPIO (circles) are shown as a function of LMD for samples having constant iron mass per cell but variable cell density (solid symbols) as well as those having constant cell density but variable iron mass per cell (open symbols). The curves for SPIO (solid line) and USPIO (dashed line) have no theoretical basis and serve only to guide the eye. Note that R_2 sensitivity to SPM is much larger for the variable cell density then the variable cell loading group despite having the same sample iron concentration for each LMD value.

Figure 1:

(a) Glass Wall (Z_0) Sample (Z_1) B_0 H_2O (Z_2)

(b) Field Map with 4 Profile Locations B_0

(c)

- Top Field Profile
- Bottom Field Profile
- Left Field Profile
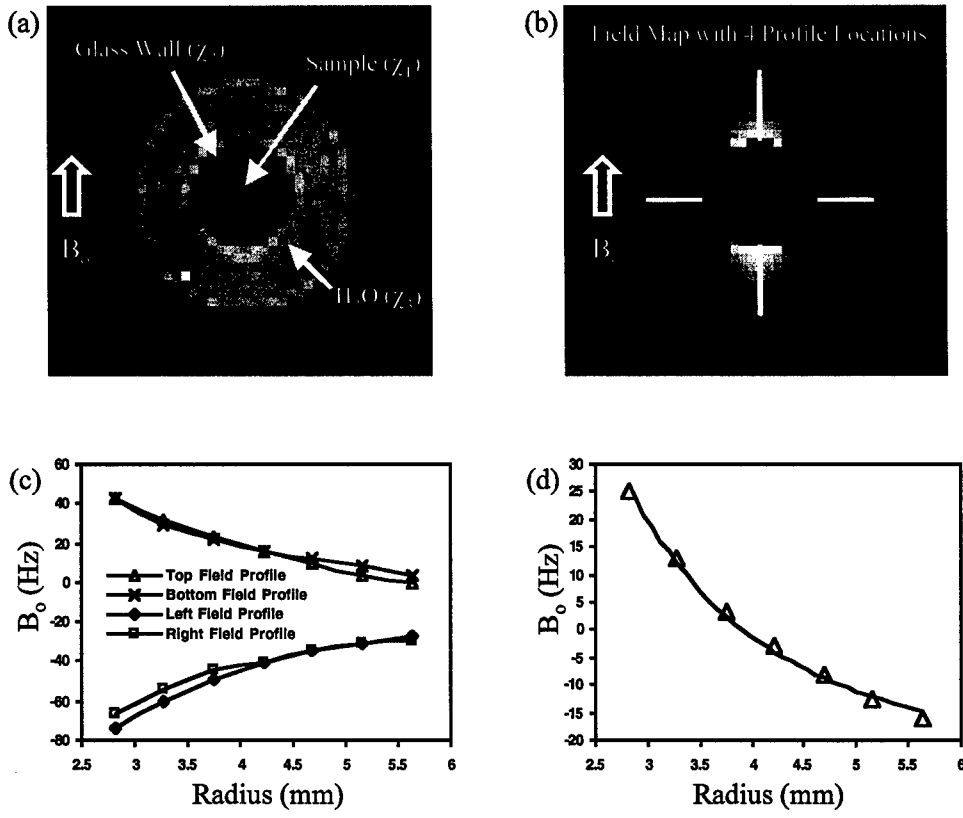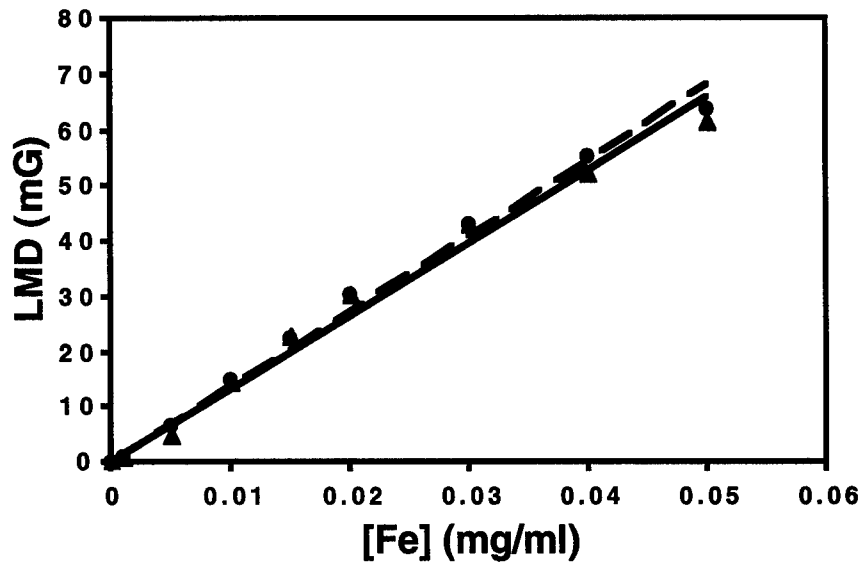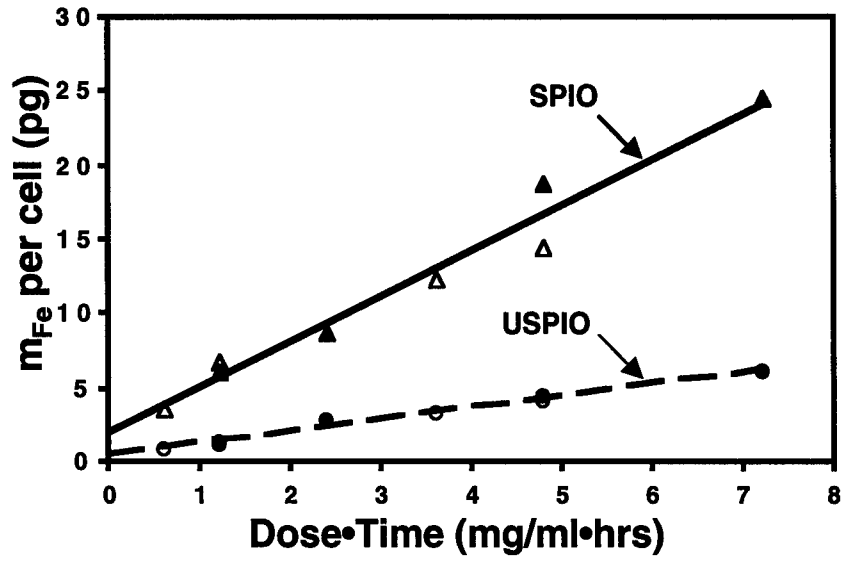- Right Field Profile

B_0 (Hz)

Radius (mm)

(d)

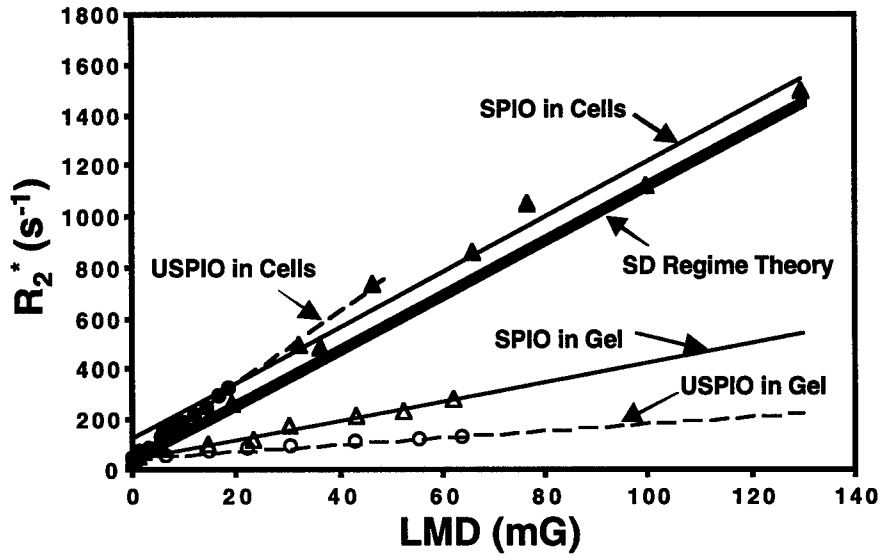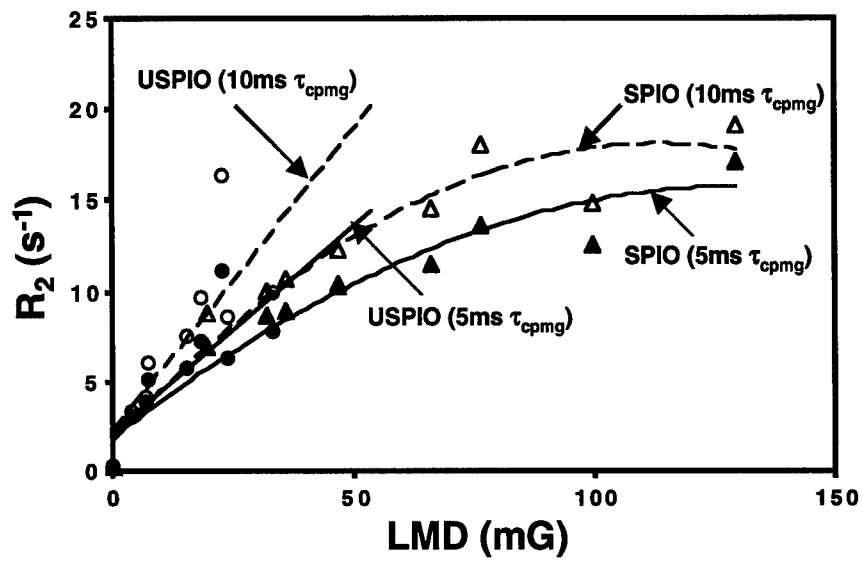

B_0 (Hz)

Radius (mm)

Figure 2:

Figure 3:

Figure 4:
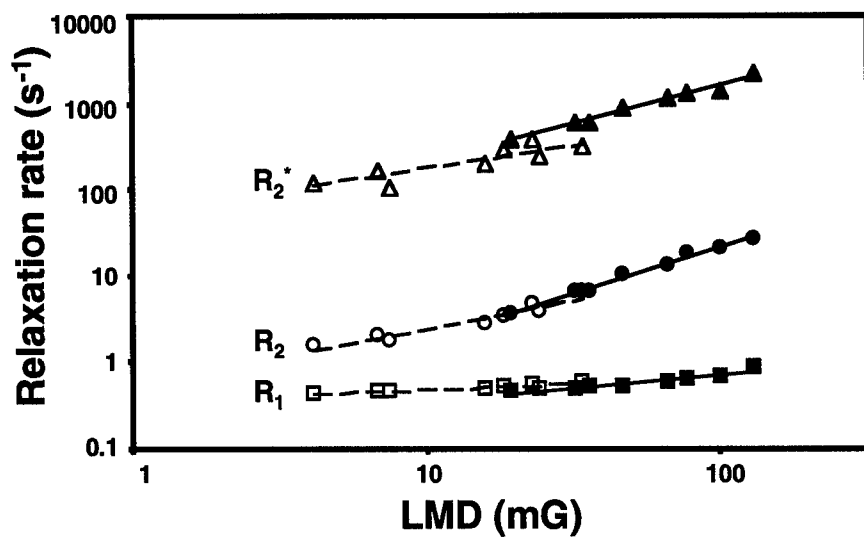
Figure 5:

Figure 6:

Figure 7:
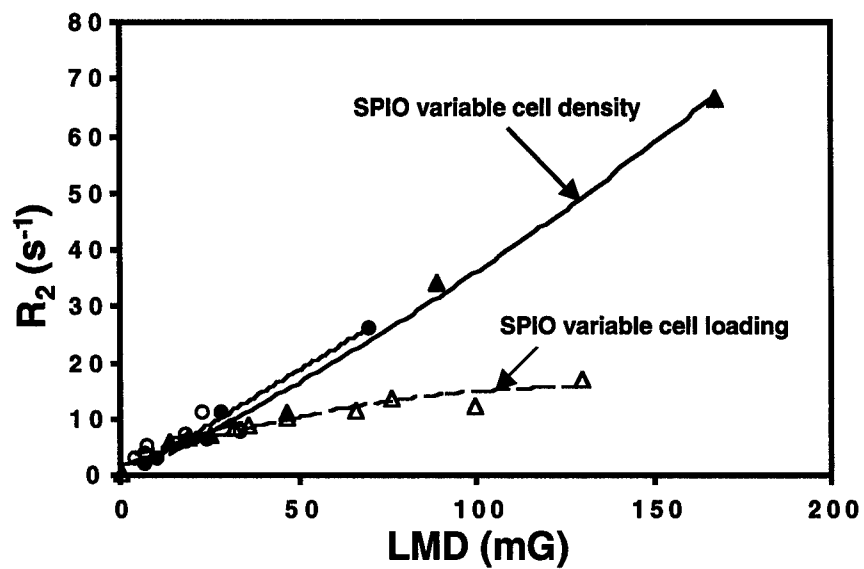
MCMR-RMI-S   (70-1y)   28 Aug 02

MEMORANDUM FOR Administrator, Defense Technical Information
Center (DTIC-OCA), 8725 John J. Kingman Road, Fort Belvoir,
VA   22060-6218

SUBJECT: Request Change in Distribution Statement

1.   The U.S. Army Medical Research and Materiel Command has
reexamined the need for the limitation assigned to technical
reports written for this Command.   Request the limited
distribution statement for the enclosed accession numbers be
changed to "Approved for public release; distribution unlimited."
These reports should be released to the National Technical
Information Service.

2.   Point of contact for this request is Ms. Kristin Morrow at
DSN 343-7327 or by e-mail at Kristin.Morrow@det.amedd.army.mil.

FOR THE COMMANDER:

Encl   PHYLIS M. RINEHART
                                          Deputy Chief of Staff for
                                              Information Management

ADB231838
ADB240253
ADB251610
ADB275099
ADB253637
ADB261538
ADB275186
ADB264648
ADB275102
ADB241899
ADB259033
ADB266113
ADB275663
ADB254489
ADB262700
ADB276708
ADB274345
ADB274844
ADB275154
ADB275535
ADB275101
ADB275451
ADB274597
ADB273871
ADB275145
ADB274505
ADB275851
ADB274459
ADB277942
ADB277404
ADB277494
ADB277536